

Titan's diverse landscapes as evidenced by Cassini RADAR's third and fourth looks at Titan

J.I. Lunine^{a,b,c,*}, C. Elachi^{c,1}, S.D. Wall^c, M.A. Janssen^c, M.D. Allison^d, Y. Anderson^c, R. Boehmer^c, P. Callahan^c, P. Encrenaz^e, E. Flamini^f, G. Franceschetti^g, Y. Gim^c, G. Hamilton^c, S. Hensley^c, W.T.K. Johnson^c, K. Kelleher^c, R.L. Kirk^h, R.M. Lopes^c, R. Lorenz^{b,2}, D.O. Muhlemanⁱ, R. Orosei^j, S.J. Ostro^c, F. Paganelli^c, P. Paillou^k, G. Picardi^l, F. Posa^m, J. Radebaughⁿ, L.E. Roth^c, R. Seu^l, S. Shaffer^c, L.A. Soderblom^h, B. Stiles^c, E.R. Stofan^o, S. Vetrozza^f, R. West^c, C.A. Wood^p, L. Wye^q, H. Zebker^q, G. Alberti^r, E. Karkoschka^b, B. Rizk^b, E. McFarlane^b, C. See^b, B. Kazeminejad^{s,2}

^a INAF-IFSI, 00133 Rome, Italy

^b Lunar and Planetary Laboratory, University of Arizona, Tucson, AZ 85721, USA

^c Jet Propulsion Laboratory, California Institute of Technology, Pasadena, CA 91109, USA

^d Goddard Institute for Space Studies, National Aeronautics and Space Administration, New York, NY 10025, USA

^e Observatoire de Paris, 92195 Meudon, France

^f Agenzia Spaziale Italiana, 00131 Rome, Italy

^g Facoltà di Ingegneria, 80125 Naples, Italy

^h U.S. Geological Survey, Flagstaff, AZ 86001, USA

ⁱ Division of Geological and Planetary Sciences, California Institute of Technology, Pasadena, CA 91125, USA

^j CNR-IASF, 00133 Rome, Italy

^k Observatoire Aquitain des Sciences de l'Univers, UMR 5804, 2, rue de l'Observatoire, BP 89, 33270 Floirac, France

^l Università La Sapienza, 00184 Rome, Italy

^m INFN and Dip. Interateneo di Fisica, Politecnico di Bari, 70126 Bari, Italy

ⁿ Department of Geological Sciences, Brigham Young University, Provo, UT 84602, USA

^o Proxemy Research, Rectortown, VA 20140, USA

^p Planetary Science Institute, Tucson, AZ 85719, USA

^q Stanford University, Stanford, CA 94305, USA

^r CO.RI.S.T.A., via J.F. Kennedy 5, 80125 Naples, Italy

^s DLR, German Space Operations Center, D-82234 Wessling, Germany

Received 28 August 2006; revised 20 November 2007

Available online 17 January 2008

Abstract

Cassini's third and fourth radar flybys, T7 and T8, covered diverse terrains in the high southern and equatorial latitudes, respectively. The T7 synthetic aperture radar (SAR) swath is somewhat more straightforward to understand in terms of a progressive poleward descent from a high, dissected, and partly hilly terrain down to a low flat plain with embayments and deposits suggestive of the past or even current presence of hydrocarbon liquids. The T8 swath is dominated by dunes likely made of organic solids, but also contain somewhat enigmatic, probably tectonic, features that may be partly buried or degraded by erosion or relaxation in a thin crust. The dark areas in T7 show no dune morphology, unlike the dark areas in T8, but are radiometrically warm like the dunes. The Huygens landing site lies on the edge of the T8 swath; correlation of the radar and Huygens DISR images allows accurate determination of its coordinates, and indicates that to the north of the landing site sit two large

* Corresponding author at: Lunar and Planetary Laboratory, University of Arizona, Tucson, AZ 85721, USA. Fax: +1 520 626 8250.
E-mail address: jlunine@lpl.arizona.edu (J.I. Lunine).

¹ RADAR Team Leader.

² Now at Space Department, Johns Hopkins University Applied Physics Lab, 11100 Johns Hopkins Road, Laurel, MD 20723, USA.

longitudinal dunes. Indeed, had the Huygens probe trajectory been just 10 km north of where it actually was, images of large sand dunes would have been returned in place of the fluviially dissected terrain actually seen—illustrating the strong diversity of Titan’s landscapes even at local scales.

© 2008 Elsevier Inc. All rights reserved.

Keywords: Titan; Radar observations; Satellites, surfaces; Geological processes; Geophysics

1. Introduction

The Cassini Titan RADAR Mapper is a K_u -band (13.78 GHz frequency; 2.17 cm wavelength) linearly polarized radar instrument capable of operating in synthetic aperture (SAR), scatterometer, altimeter and radiometer modes. Here we report on data acquired during two early passes, referred to as T7 and T8, on September 7 and October 28 (Universal time dates), 2005, respectively. In contrast with the previous Ta and T3 opportunities, these were southern hemisphere passes, and in particular, T7 imaged areas at high southern latitude (Fig. 1 and Table 1). T7 comprises an area less than a third that of T8 (0.6% versus 2% of Titan’s surface) in part because a problem external to the radar interrupted onboard recording of the T7 data after the midpoint of the pass.

In this paper we compare the two radar passes, which are strikingly different in terms of terrains and radiometric properties, extend the maps of radar units developed from Ta and T3 in another paper (Stofan et al., 2006), and infer the nature of processes that formed various features. While the most striking and recognizable structures in Ta and T3 are, respectively, a volcanic edifice (Lopes et al., 2007) and two impact craters, the dominant recognizable features in T7 and T8 are, respectively, channels and dunes.

As in the first two passes, there are large areas of enigmatic and ambiguous terrains in both T7 and T8. By combining results from radiometry and synthetic aperture imaging (SAR), it is possible to compare the dark dune terrain and the smooth, apparently dune-free dark area at the south end of T7 in terms of material properties (Paganelli et al., 2007). The two passes, paired by proximity of their flyby dates, could not be more different from each other; they reinforce the impression from earlier flybys that Titan’s surface is worked by a range of geologic processes, not dominated by one in particular, and in this respect is much like Earth.

In this paper, we consider first the morphologies seen in the SAR imagery from T7 and T8, in Section 2 drawing a general picture of the nature of each region and in Section 3 considering in more detail the variety of features evident in the T7 and T8 SAR imagery and the processes that might form them. In Section 4 we review the evidence from radiometric data that the T7 dark plain is similar to the dune fields seen in T3 and T8, and use this along with the radar properties units identified in Stofan et al. (2006) to delve deeper into the nature of the T7 dark area in particular. In Section 5 we discuss how DISR data and radar data were overlaid to identify the Huygens landing site in T8 SAR imagery. Section 6 provides a comprehensive interpretation of the processes shaping the T7 and T8 swaths, and closes

Table 1
Swath characteristics

| | T7 | T8 |
|--------------------------|-----------|-----------|
| Resolution range, km | 0.3–0.8 | 0.3–1.2 |
| Acquisition date | 7-9-05 | 27-10-05 |
| Swath length, km | 1970 | 5000 |
| Latitude range, ° | 31–70 S | 11–7 S |
| Longitude range, ° | 23 W–11 E | 186–314 W |
| Incidence angle range, ° | 15–30 | 17–23 |

with questions raised by the two passes that will need to be addressed by future data sets

2. Description of T7 and T8 terrains

The two swaths are displayed as a set of quadrangles in Fig. 2 (T7) and Fig. 3 (T8). The full swaths are, at the time this paper goes to press, released in various formats on the Planetary Data System home page.

2.1. T7

The swath begins in the mid-southern latitudes (31° S, 23° W) and proceeds in a south- to southeasterly-direction for some 1970 km to latitude 70° S and longitude 11° E. Illumination of the swath is from the upper long-side of the strip (when laid out in landscape orientation) downward, that is, roughly toward the southwest. The image resolution begins at about 740 m, improving to 300 m in azimuth and 450 m in range at the poleward end of the strip near closest approach. The asymmetric nature of the resolution, in contrast to other passes, is an artifact of the loss of the second half of the radar pass. The strip width is 304 km at the equatorward end, and 113 km at its narrowest point.

An area of moderate radar reflectivity characterizes the equatorward edge of the strip and presents a mottled appearance with faint circular features that seem more characteristic of T8 than of the rest of T7. This terrain quickly gives way to a complex of topographically elevated features distinguished by the obvious illumination and shadowing associated with the radar beam (Fig. 2a). These “hills” are arranged in a roughly semicircular fashion around an area of roughly two or three thousand square km. The lack of closure of the hills to the north, the presence of a similarly incomplete but much smaller (roughly 8 km diameter) oval toward the middle, and the lack of distinct topographic features in the darker material enclosed by the semi-circle, suggests that the hills are the remnant of a more extensive structure that has been partially buried and/or eroded. The debris responsible could have been eroded off the hills by

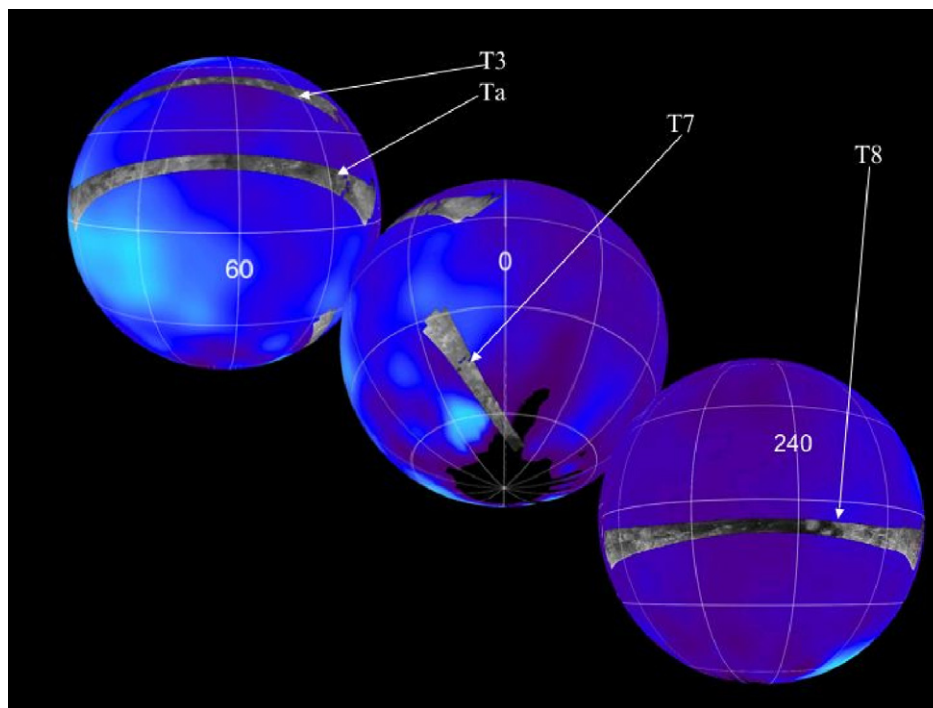


Fig. 1. Globes of Titan showing locations of Ta, T3, T7 and T8 data swaths. The swaths are superposed on globes composed of false color images from the Hubble Space Telescope. White lines indicate 30 degree latitude and longitude markers. 60°, 0° and 240° longitudes, respectively, are indicated. The top globe shows the Ta and T3 swaths, the middle globe shows the edge of the T3 swath and the T7 swath, and the bottom globe shows the T8 swath. North is up, and west longitude is used. See Table 1 for exact locations and dimensions of the T7 and T8 swaths.

rainfall, as is seen at the Huygens landing site in DISR images (Tomasko et al., 2005), or deposited as sedimenting aerosols. The fact that the radar-dark material is not very radar-dark compared with that seen in parts of other swaths (Elachi et al., 2005) hints that the overall terrain may be fairly rough, consistent with but not requiring an erosional interpretation (for example, unconsolidated aerosols directly deposited from the atmosphere might be radar bright as well).

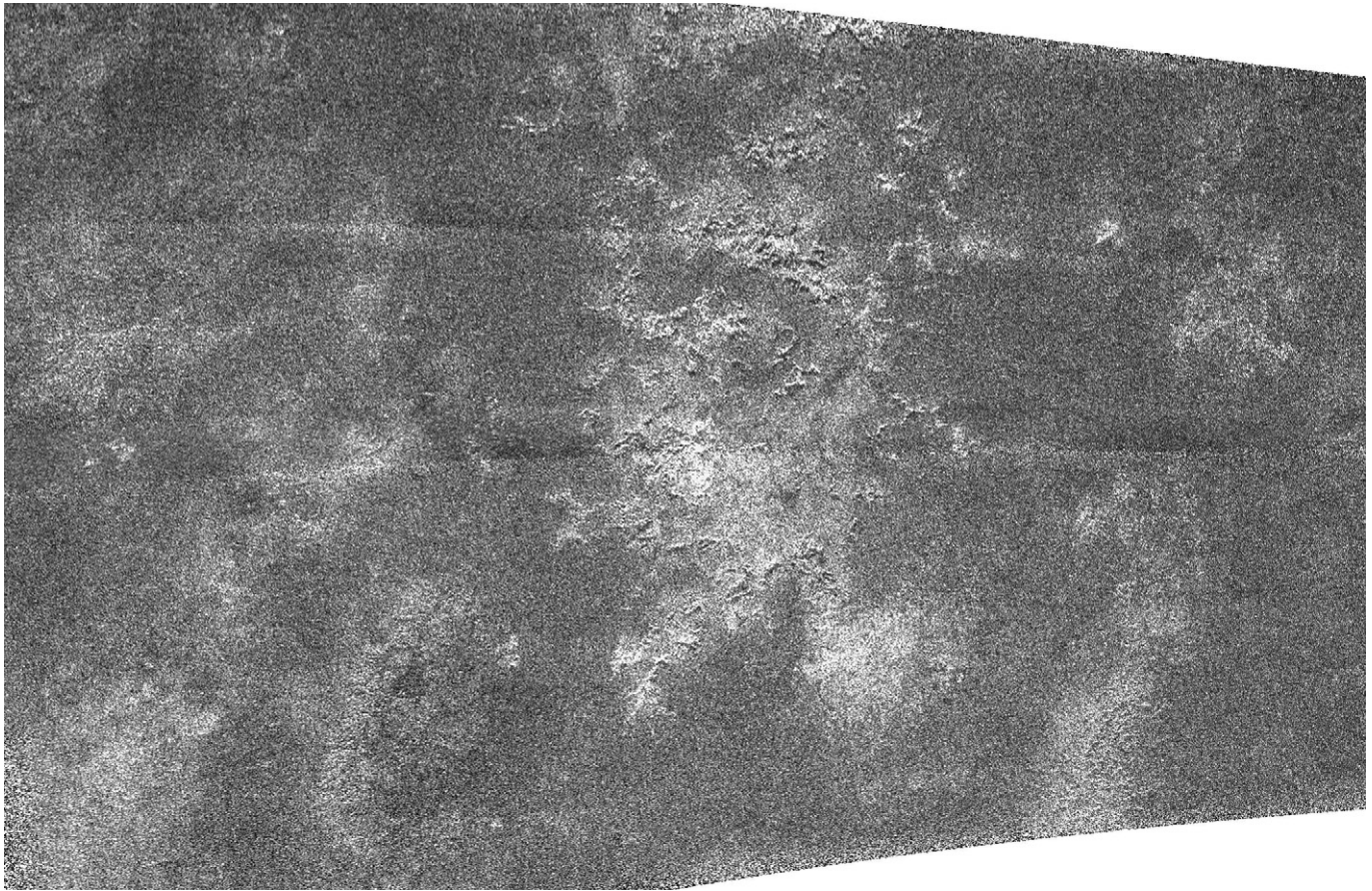
Proceeding poleward, past a break in the radar strip on the edge of which may be another (but more poorly defined) circular set of hills, the landscape becomes dissected by a set of channels running roughly poleward from 45° S. The radar return is brighter where the channels fan out more extensively, suggesting deposition of debris (Fig. 2b). The brighter debris fields seem to be truncated by some process—perhaps a change in topographic gradient—that is not evident in the images, so that the terrain becomes radar-dark (and hence possibly smoother) again. Beyond the dark region, however, more channels appear. In some cases channels can be traced for hundreds of kilometers through the transition from darker-to-brighter-to-darker terrain, but there are few of these features, and their courses seem independent of the fan-shaped channel systems (Fig. 2c).

At about 55° S more numerous channels are located in an irregularly shaped bright area of roughly 40,000 square km with no apparent topographic control, against which the channels become dark and appear to broaden out (Fig. 2d). Dark patches, each about 10 km in linear extent and separated by smaller, very bright spots, exist along the western margin of the bright area; the contrast between the dark patches and the bright spots is the largest in T7 and among the largest in any of the four passes

to date. The bright spots have the appearance of being topography illuminated by the beam, but if these are hills they are not organized in any obvious fashion.

The bright area ends southward of 60° S latitude in a terrain with a faint east–west trending texture, the latter continuing poleward about 40 km into a dramatic landscape of semicircular, scalloped terrain that eventually is embayed by a darker, very subtly modulated terrain (Fig. 2e). This dark area is the part of the radar swath with the highest resolution, yet no well-defined features can be seen beyond a subtle, patchy variation in brightness. The brighter highlights in the scalloped terrain might be hills of relatively low relief that outline the topographic impediments to the dark terrain, a change in abundance of cm-scale pebbles, or other variations. In the absence of clear slope effects, or more generally topographic data, it is impossible to decide among these possibilities. It may also be that the scalloped terrain extends further equatorward than is apparent in the images, because it has been partially buried by the material in Fig. 2e with the east–west trending texture.

The overall impression generated by the T7 data is that of a landscape that is descending in elevation toward the pole, dissected by rain- or spring-fed fluvial channels, and ending in a now- or recently-wet high-latitude basin bordered by scalloped and embayed terrain. Basic physical conditions in Titan's atmosphere (Fulchignoni et al., 2005), the meteorological conditions at the Huygens landing site (Niemann et al., 2005), and the appearance of the channels themselves as being cut by low viscosity fluids argue for liquid methane, or secondarily liquid ethane, as the working erosive fluid in the channels and—if wet—the dark, nearly featureless terrain closest to the pole.



(a)

Fig. 2. Various views from the T7 SAR pass, shown progressively from the equator toward the pole. (a) Semi-circular pattern of hills. Image area is roughly 250×420 km. The image is centered at 340.7° W, 39.9° S. (b) Area in T7 cut by fairly extensive fluvial channel, fanning out into rougher (brighter) terrain. Image area is roughly 170×280 km. The image is centered at 345.5° W, 47.6° S. (c) Trace of one fluvial feature appears to run across the bright fan on the left, extending all the way across the 400 km length of the image. The image is centered at 347.5° W, 52.3° S. (d) Transition zone into a region of broader channels seen against a bright (rough?) background. Image 150×450 km, with resolution approaching 400 m. The image is centered at 352.4° W, 57.3° S. (e) Most poleward and highest resolution part of the T7 swath, showing the transition from a scalloped terrain to a dark, almost featureless plain. Image size 150×490 km. The image is centered at 3.4° W, 66.6° S. (f) Blow-up of the scalloped terrain. The image is centered at 3.4° W, 66.6° S.

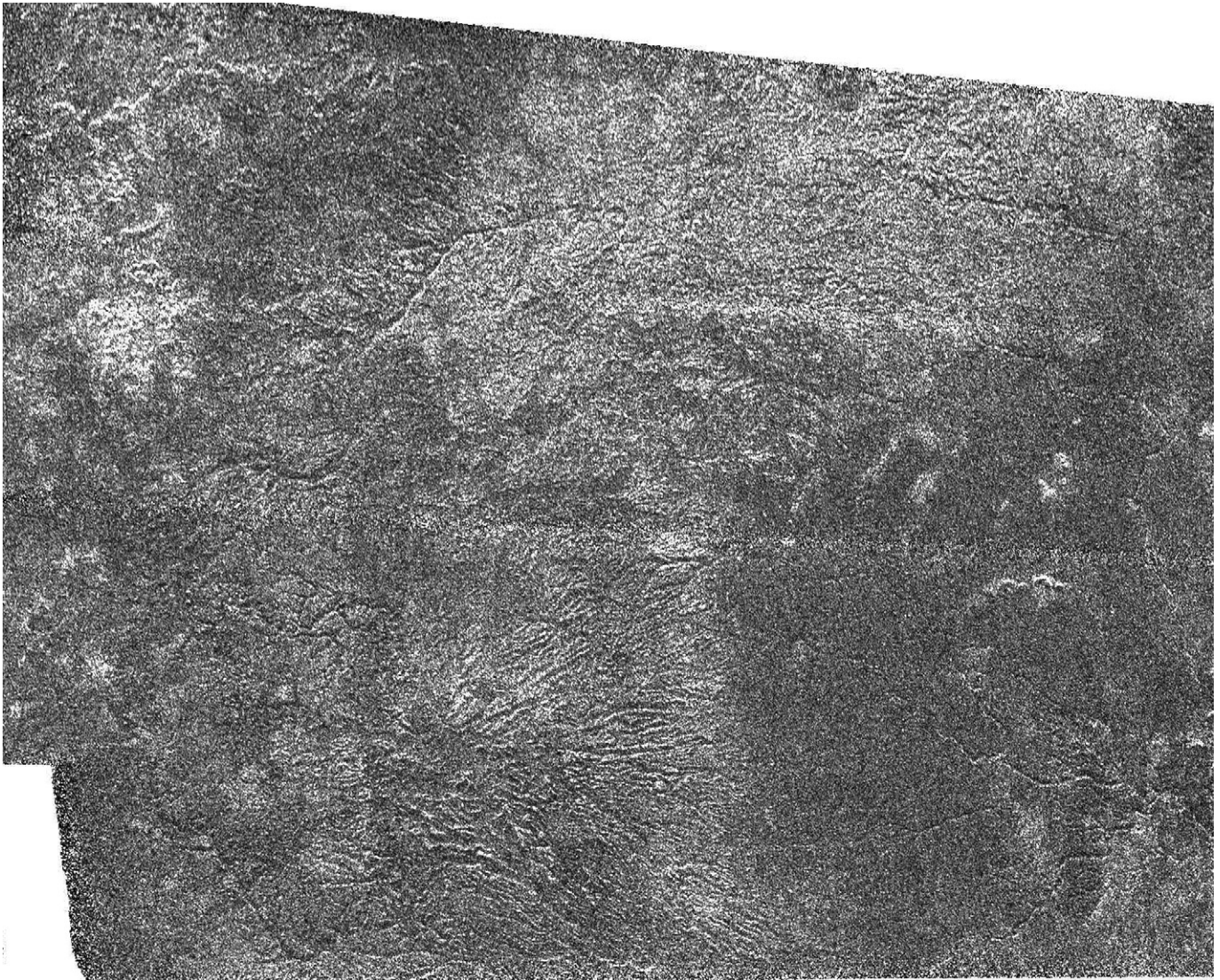
2.2. T8

This swath spans over three times the surface area covered by T7, and presents a very different set of geologic features. The swath progresses east some 5000 km from longitude 186 to 314° W, over a latitude range from 11 to 7° S. Illumination of the swath is from the top of the strip downward, that is, toward the south, with an incidence angle of the radar beam varying between 18° and 20° near the center of the pass. The image resolution is about 1 km at each end of the strip, improving in the center to 300 m in azimuth and 450 m in range. The swath width is 450 km at the usable ends, narrowing down to 180 km near the midpoint of the acquisition.

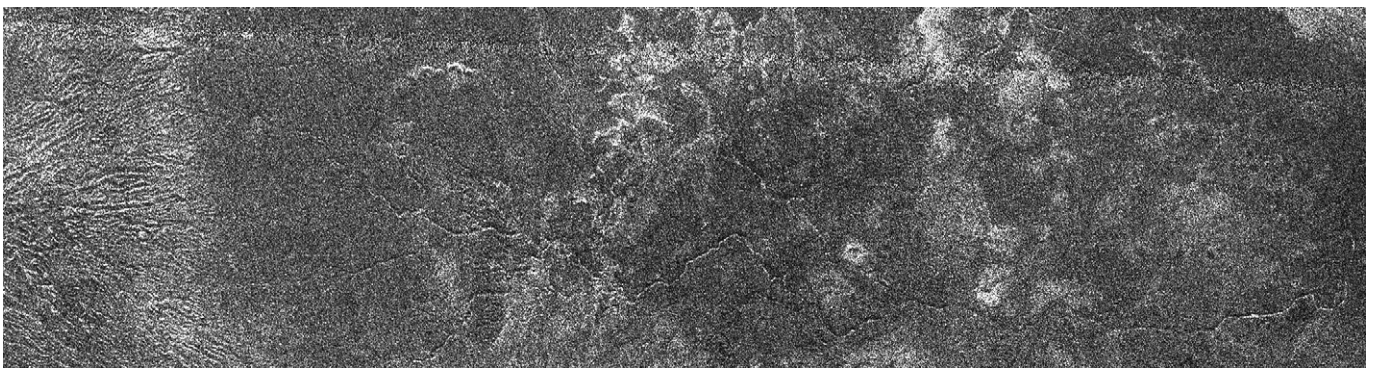
The western edge of the swath consists of a poorly defined set of bright and dark patches, within which radar-dark, longitudinal dunes (Lorenz et al., 2006) become increasingly apparent toward the east. The contrast between brighter and darker patches increases as well, although it is not clear whether this is an artifact of the decreasing distance of the radar from Titan both improving the spatial resolution and decreasing the

noise in the image, or a real surface contrast. A few very dark, short channels seem to cut across some of the brighter terrain (Fig. 3a). About 1400 km east of the start of the swath, an extensive area of dark, regular dunes appears (Fig. 3b). These dominate the landscape, parting and rejoining around isolated bright obstructions in the field for some 1700 km until they are interrupted by two obstructions each about 100 km in extent (Fig. 3c). To the east of these lies perhaps the most enigmatic area in the two SAR strips. A series of roughly east–west trending hills, whose topographic amplitude from radarclinometry ranges up to 1800 m (Radebaugh et al., 2007) are interspersed with a variety of vaguely circular features and dark, dune-filled basins (Fig. 3d). East of this terrain are a few faint fractures or fluvial channels (Fig. 3e), beyond which more extensive dune fields resume again near the northeastern end of the pass.

The overall impression of the T8 region is that of a much less coherent set of morphological signatures than in T7, although this could be an artifact of the much greater areal extent of T8 compared to T7. It is clear that, in the equatorial 2% of Titan covered by T8, fields of longitudinal dunes dominate



(b)

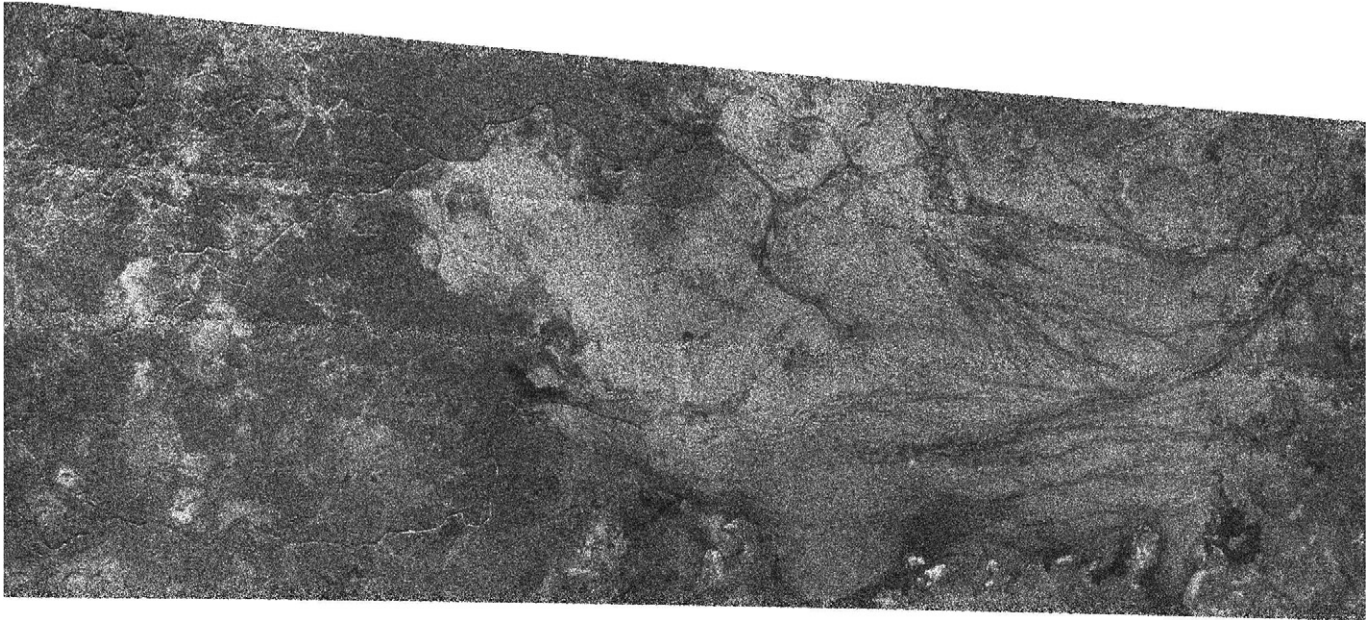


(c)

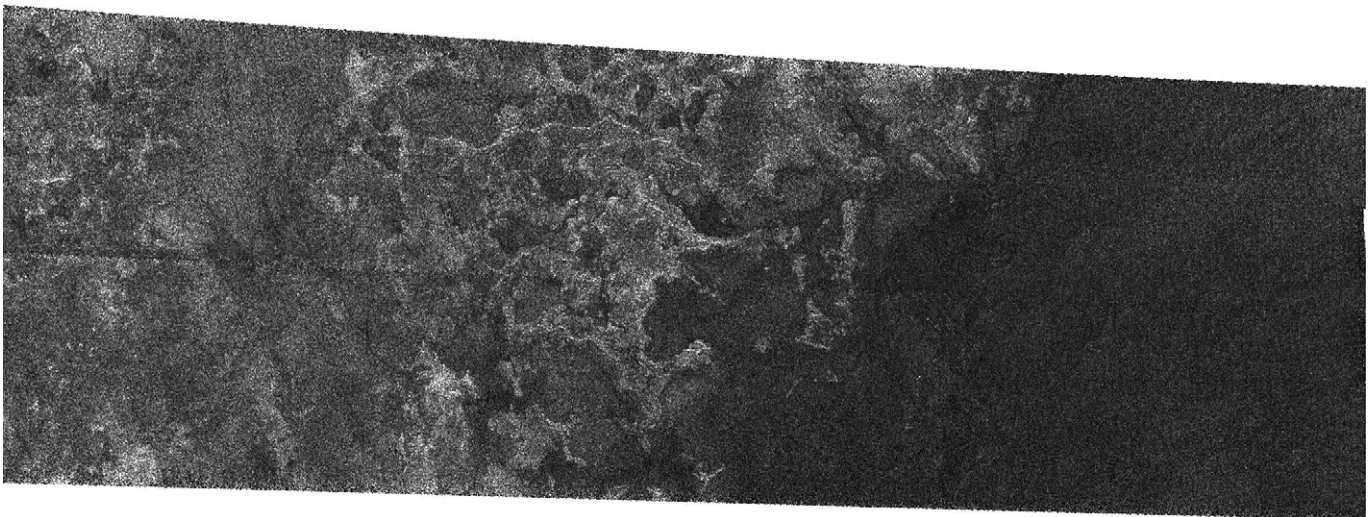
Fig. 2. (continued)

(Lorenz et al., 2006). But what is unclear is the geological origin of the crustal structures that are partly buried by the dunes. The circular features east of the main dune field have a variety of morphologies, some seemingly associated with the hilly topography, others not. Some appear to be partly buried. The

largest, which is well to the east of the ridges, possessing a diameter of roughly 60 km, is not much smaller than the impact crater Sinlap (Elachi et al., 2006), and yet exhibits none of the crisp topography and contrast that the latter possesses. Specific morphological differences between these circular fea-



(d)



(e)

Fig. 2. (continued)

tures and previously identified impact craters include lack of a well-defined rim or surrounding ejecta blanket.

The end of the T8 radar swath includes the Huygens landing site. Colocation of the Huygens DISR and radar data provided a definitive set of coordinates for the site of 10.2° S, 192.4° W. The collocation process depended on the existence of a set of well-defined dunes in the radar strip also seen in DISR imagery; see Section 5.

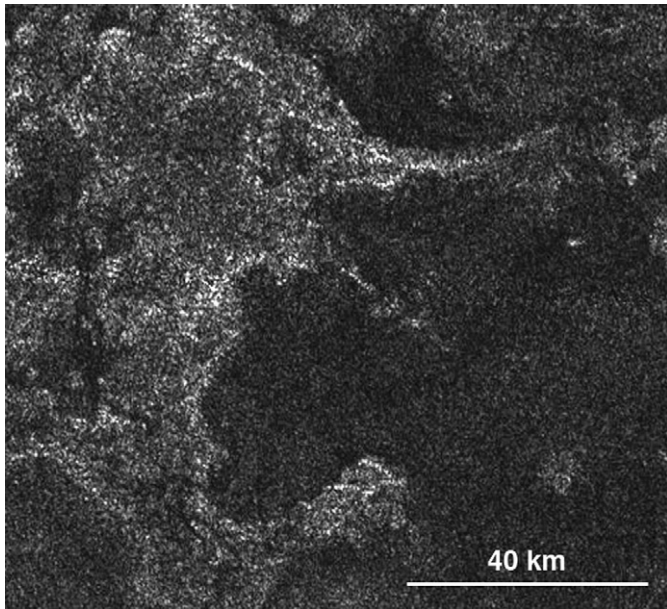
3. Processes seen in the T7 and T8 data sets

In this section we consider a variety of processes previously identified in radar passes (Elachi et al., 2005, 2006), VIMS data (Sotin et al., 2005), and Huygens DISR imagery (Tomasko et al., 2005). In some cases, identification of features with a particular process is provisional or ambiguous, and may remain so

until higher resolution data become available from future missions.

3.1. Fluvial features

Prior to the Huygens probe descent, the Cassini RADAR detected potential fluvial features on the October 2004 Ta encounter at around 50° N. This first SAR image of Titan's surface showed some narrow, radar-bright, sinuous features a few tens of km long and less than 1 km wide which were interpreted as possible canyons (Elachi et al., 2005). In two cases joining with bright triangles that may be alluvial fans. Such an interpretation appears consistent with the striking observation by the Huygens probe (at about 10° S) of rounded cobbles at an apparently alluvial landing site (Tomasko et al., 2005) and of fluvial networks with channels some tens of meters across and around



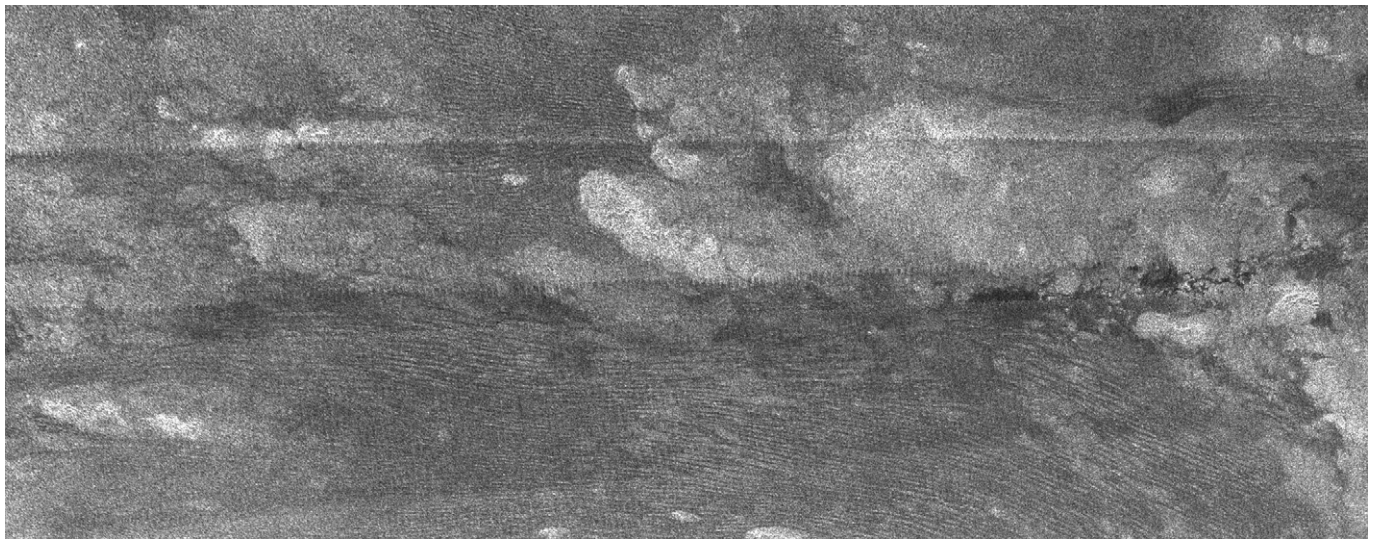
(f)

Fig. 2. (continued)

10 km long. In both the above sets of features, the orientations appeared to be controlled by local hillside slopes.

Rather larger fluvial networks (one sparse and dendritic with channels a few km across, and another denser, braided network) up to 200 km long were observed on T3 (Elachi et al., 2006) at latitudes of about 20° N. Both networks, on either side of the Menrva impact structure, appear to flow in a northeasterly direction, away from the broad, bright region Xanadu, hinting at a possible regional slope. All of these channels appear shallow in the images, like desert washes or wadis, lacking any apparent topographic expression (although the radar's limited spatial resolution could admit possible incision depths of a few tens of meters).

In sharp contrast, in T7 a number of rather deeply incised channels are observed. One region, around 40° S is characterized by a dense network of channels, while further south, one or two channels make their way southeastwards towards the 'shoreline.' Radarclinometry suggests the channels in T7 may be up to 100 m deep with fairly consistent widths; that is, they do not seem to be the large-scale end of a cascade of channel sizes that extend to below the radar resolution of roughly $1/2$ km. It is noteworthy that the orientation of the channels is

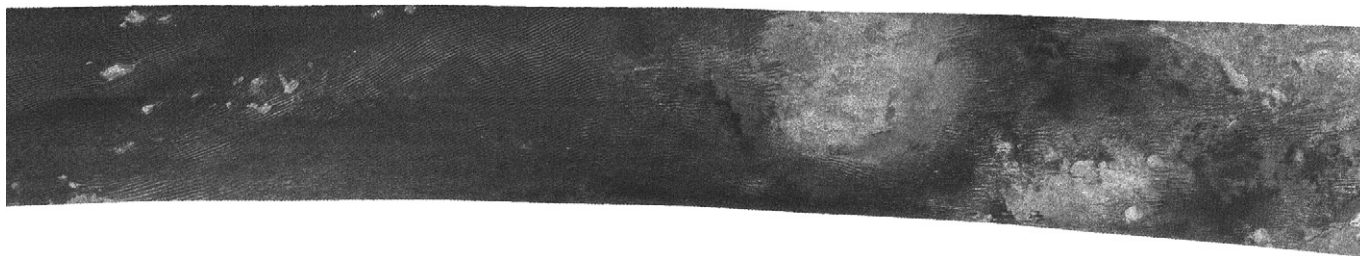


(a)

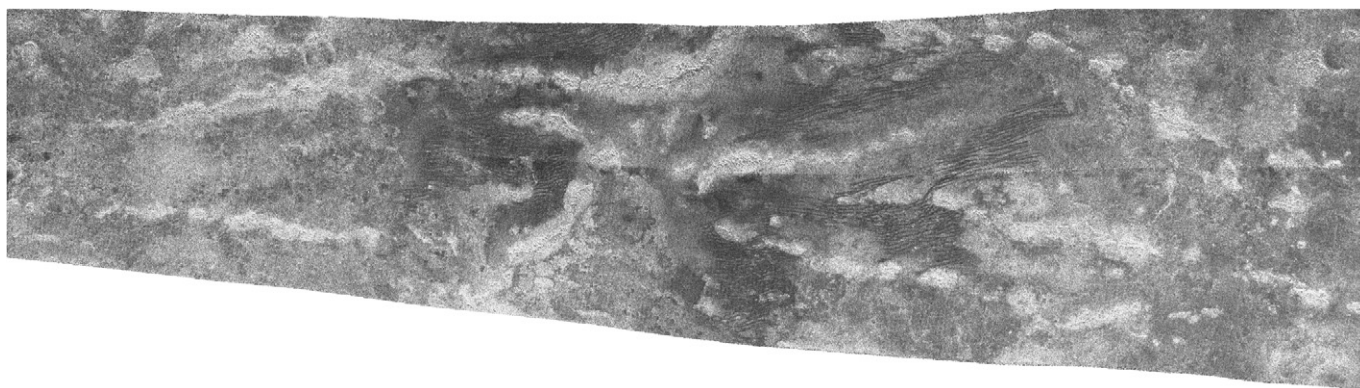


(b)

Fig. 3. Various views from the T8 SAR pass, moving from west to east across Titan just south of the equator. (a) Relatively low (1 km) resolution view showing some poorly organized dunes, and dark, possibly fluid-filled, channels. Image area 300×600 km. The image is centered at 59.3° W, 8.53° S. (b) Onset of the well-organized dune fields near the center of T8, seen at very high (300–500 m) resolution. Image size 150×1000 km. The image is centered at 93.7° W, 8.0° S. (c) Dunes part and rejoin around obstructions, in the area east of the previous image. Image size 210×850 km. The image is centered at 119.7° W, 7.2° S. (d) Enigmatic terrain in which a series of ridges are interspersed with circular features of varying contrast. Area is 270×800 km. The image is centered at 145.6° W, 8.8° S. (e) Near the eastern end of the T8 swath, a large but faint circular feature is seen at low (1 km) resolution south of where another extensive dune field begins. Area 380×440 km. The image is centered at 164.7° W, 10.1° S. (f) Blowup of the dune terrain, showing in more detail the parting of the longitudinal dunes around a presumed topographic obstruction. The image is centered at 108.9° W, 6.4° S. (g) Blowup of the termination of a dune field against what appear to be several mountains. The image is centered at 143.7° W, 8.6° S.



(c)



(d)

Fig. 3. (continued)

consistent with that of T3, in the sense of being toward the east and the pole, and therefore away from Xanadu.

In a couple of locations, the channels are rather straight, in one case appearing to form a boundary between a generally radar-brighter substrate to the west and a slightly darker region to the east. Such a straight edge suggests some sort of structural control on the channel.

Dendritic features of another character, broad and radar-dark, were seen further south (poleward) in T7. It is not possible to determine whether they are channels, because no topographic expression is visible; they may even be slightly built-up or leveed flows. The radar-dark but speckled appearance suggests they are smooth. Therefore it is tempting to speculate that these are distributary channels that have deposited material that was chiseled out of the channels closer to the equator. The fine-grained materials created in this process may also be a source of the ‘sand’ forming the dunes.

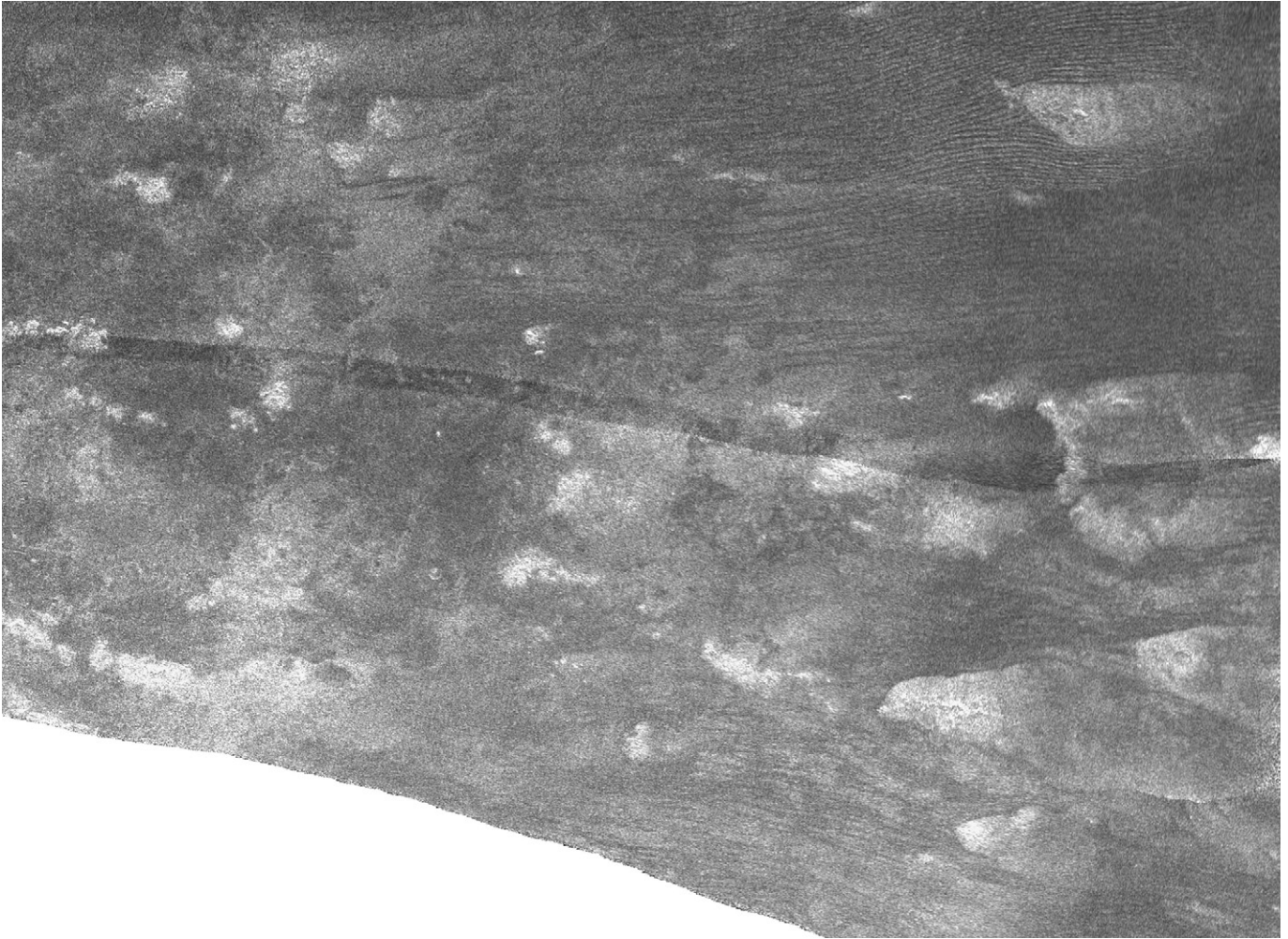
The T8 swath, between about 5° and 12° S, presents an altogether different picture, with essentially no fluvial features at all. A couple of short, narrow, potential channels are suggested, but these show no consistent pattern of orientation or association with other features. The segment of the T8 swath covering the Huygens landing site is of relatively poor resolution (~1 km) and the channels observed by Huygens could not be detected.

The fluvial features observed to date and their meteorological context are discussed in more detail elsewhere (Lorenz, 2006), though it is worth mentioning that the most prominent fluvial features are found at midlatitudes, where the global circulation model (GCM) of Rannou et al. (2006) suggests massive (terrestrial day-long, covering 5% of Titan’s disk) methane storms during summer.

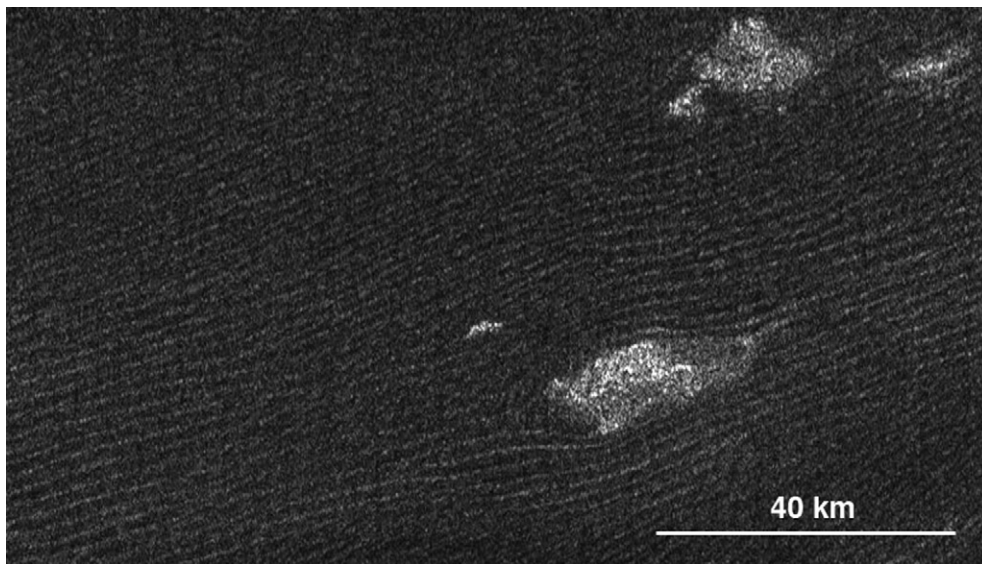
3.2. Lacustrine features

T7 brought the highest-latitude SAR coverage to date. At high southern latitudes, the character of the surface changes profoundly from a somewhat bright region dissected by the various channels described above to a nearly uniformly dark region. The boundary between them appears scalloped and cusped, like that of some estuarine shorelines on Earth. Unfortunately, the premature truncation of the T7 data collection prevented seeing the poleward boundary of the feature. The morphology of the dark region suggests it to be a smooth plain or a basin.

However, if it were filled with liquid to a significant depth, the dark region should be even darker than observed. In fact, this region is comparable in darkness to the band plains in the northern midlatitudes and slightly brighter than the main dune fields. Quantitative comparison of the dark region with two of the largest northern hemisphere lakes seen in T25 (Mitchell et al., 2007) shows that the T7 dark area is at least 10 dB brighter than either. (This is a lower limit to the brightness difference since much of the area in the two T25 features sits roughly at the noise floor.) Analysis of the microwave absorbing properties of liquid methane and ethane suggests that if the northern hemisphere lakes contain pure ethane–methane liquid (without more absorbing solvents or suspended debris), their darkness implies a significant physical depth, greater than tens of meters at least, or they are underlain by sediments that suppress bottom reflection through resistive loss or some other process. It is thus possible that the appearance of the T7 dark area, with its very subtle features, is due to a shallower layer of liquid methane and ethane. Such an hypothesis, of an exposed but shallow area of liquid, could be tested with additional flybys at different radar



(e)

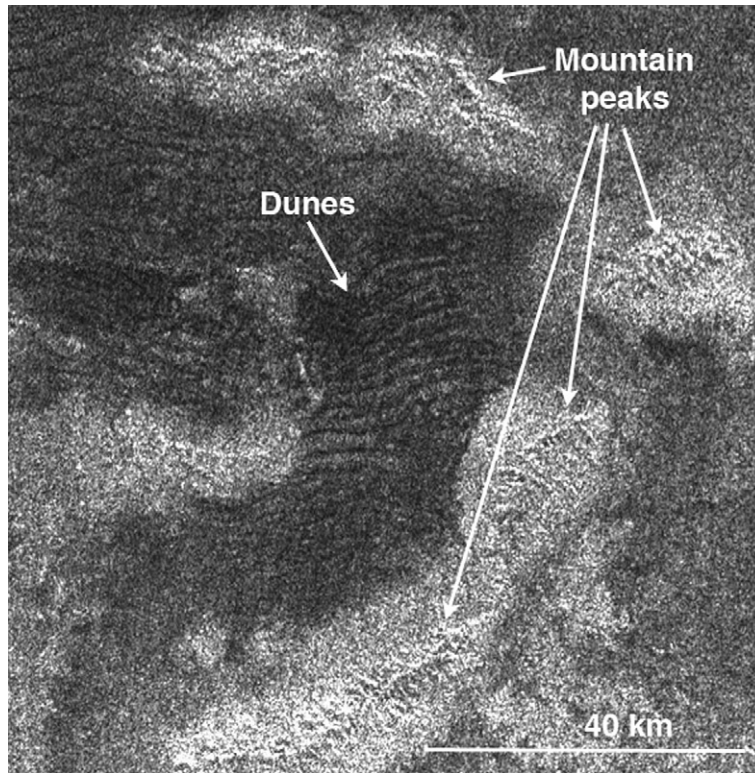


(f)

Fig. 3. (continued)

azimuths, and evaluated in terms of the potential excessive tidal dissipation such a broad shallow sea would have on Titan's orbital eccentricity (Sears, 1995).

The alternative, given that the low reflectivity of this terrain is unremarkable compared even to the dunes, is that it is completely dry but contains small variations in particle size or



(g)

Fig. 3. (continued)

even composition that produce the subtle features we see. However, this area is smoother than the Huygens landing site, which appears quite bright in the SAR image of the landing site and based on the DISR images (Tomasko et al., 2005) is a pebble strewn plain or deflated dry lakebed.

3.3. Aeolian features

No dunes were observed in T7: these linear, radar-dark features were observed in several large (hundreds of km) patches in T3, and were suspected to be aeolian in origin (Elachi et al., 2006). However, the T8 swath, over a near-equatorial area known to be optically dark, found aeolian features in striking abundance. As documented in Lorenz et al. (2006), over half the swath was occupied by linear (longitudinal) dunes, very similar in size and morphology to those found on Earth in the Arabian and Namib deserts. In much of the swath the high viewing geometry (orthogonal to the long axes of the dunes) permitted topographic shading to appear, suggesting dune heights of ~ 150 m and slopes (averaged over ~ 350 m pixels) of about 6° .

The longitudinal nature of the dunes is evident from their interaction with other topography—the dunes break around and rejoin beyond topographic obstacles such as the hills or mountains on the eastern end of T8 (Fig. 3f). Such a morphology requires a fluctuating (typically bidirectional) wind regime—Lorenz et al. (2006) suggest that the gravitational tidal winds modeled by Tokano and Neubauer (2002) may be responsible for the variation, although the general trend of the dunes is eastwards, consistent with the zonal winds at high altitudes. A

systematic mapping of the dune orientation in future work will be an important constraint on Titan's wind meteorology. It is already apparent that there are regional deviations from the generally eastward trend, in some cases by as much as 30 degrees. In most cases these deviations can be attributed to the influence of nearby topography, and in one prominent case, a set of transverse dunes appear where a topographic obstacle appears to 'straighten' the fluctuations in flow direction (Radebaugh et al., 2008).

The dunes appear superposed on all other features, suggesting they are relatively young. It is estimated (Lorenz et al., 2006) that formation times may be as short as a few thousand years, similar to terrestrial dunes. Optically dark (and radar-dark) areas at low latitudes often appear to be associated with dunes. However, at higher latitudes thus far observed, dark regions are apparently due to something else—either sand sheets not sculpted into dunes, or perhaps liquid deposits.

3.4. Hills

Features with high topography above surrounding terrain within the T7 swath include a cluster of hills at the northwestern end of the swath and high plateaus within the middle, radar-bright, dissected region. The northern hills are most likely the remnants of a partially buried, eroded structure, perhaps a sub-circular volcanic ring or impact crater. However, the structure is so eroded that it is difficult to confidently propose any particular mechanism for its origin. The central, radar-bright region contains channels that appear to have cut down through under-

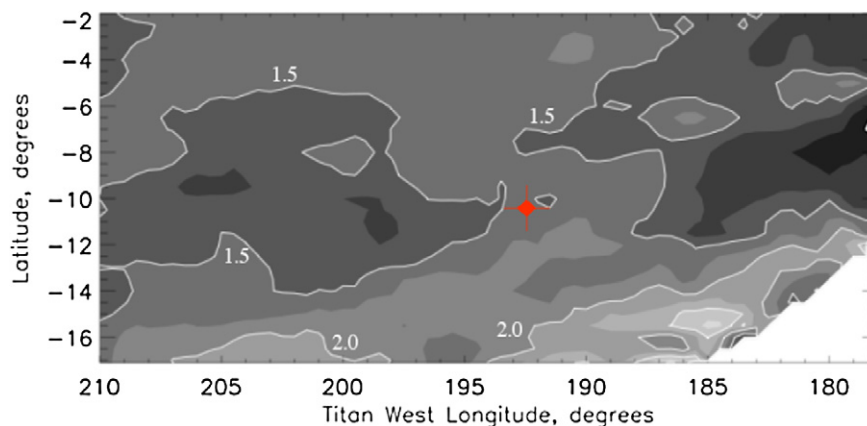


Fig. 4. The dielectric constant of a region containing the Huygens probe landing site retrieved from orthogonally polarized radiometer measurements taken during the Ta and T8 passes. The shading shows dielectric constant ranging from low (dark) to high (light). Contour levels for dielectric constant = 1.5 and 2.0 are identified. The location of the Huygens probe landing site is shown by the red diamond.

lying materials. There is some evidence of topography in the form of bright/dark pairing associated with the channels, perhaps similar to the channeled regions seen by Huygens DISR near the landing site (Kirk et al., 2005), but on a much larger spatial scale. The gradation southward to channels that show no evidence of topography suggests a crude analogy with the Colorado Plateau, in which rivers erode through bedrock, leaving steep cliffs that grade to gentle alluvial fans.

The eastern end of the T8 swath, just west of the Huygens landing site, contains long chains of features demonstrating high topography through radar shading that have been described as mountains (Radebaugh et al., 2007). These features are curvilinear in planform, have an overall E–W orientation, and form ranges that extend several hundred kilometers. They have a strong appearance of having experienced erosion, both in their disconnected summits and in the light colored, diffuse materials (perhaps erosional blankets) that surround the mountains. Strong bright/dark pairing between the mountain summits enabled us to use radarclinometry to calculate slopes and heights of various peaks within the ranges. Maximum mountain heights are just under 2000 m (with a mean of 930 m) above their surrounding blankets, and mean 90th percentile maximum slopes are close to 10 degrees (Radebaugh et al., 2007). The curvilinear morphology of these ranges indicates they may have formed through some type of volcanic activity. Localized compression of the crust is a possibility, due to the thickening of Titan’s water ice crust associated with general cooling or, very recently, the onset of crustal convection (Tobie et al., 2006).

3.5. Circular features: impact or cryovolcanic?

Small bright-rimmed, dark floored circular features—what we call here “ink spots” to characterize their distinctive size and reflectivity—are common in the T8 swath (see the figures in Wood et al., 2006 and Lopes et al., 2007). Their diameters are generally only 1–10 km, which assuming an impact origin is at or below the limit expected based on the screening effect of the present-day atmosphere (Lunine et al., 2005). Each feature is poorly resolved but as a class they seem distinctive. The fea-

tures are quite round and often have narrow bright rims. More than 500 such circular features were observed in the T8 mountains region, covering 800×200 km. They present a dark center with brighter rims with diameters generally ranging between 1 and 2 km, and a steep decline toward higher diameters.

Two hypotheses can be proposed to explain the origin of these ink spots: impact craters or cryovolcanic features, either collapse or explosion pits (Lopes et al., 2007) or hydrothermal vents. The general paucity of much larger and hence more readily recognizable impact craters on Titan (Elachi et al., 2006), and the improbable size distribution of these features (impactors responsible for craters of this size, 1–2 km, should not be able to pass through the atmosphere without breaking up given the column density of Titan’s atmosphere; Lunine et al., 2005), argues against a primary impact origin. The absence of larger features nearby that could be interpreted to be impact craters militates against an origin from secondary impacts, although we cannot rule out completely the possibility of primary craters adjacent to the T8 strip, which is isolated from other SAR strips obtained to date.

Heating of methane pockets by subsurface cryomagmas might cause explosive (“cryoclastic”) activity, leading to formation of volcanic pits such as the ink spots. Alternatively, methane released from a subsurface reservoir hundreds of meters under the surface might lead to fluidized sediments and/or ice expulsion along conduit tubes terminating at Titan’s surface as numerous small circular pits. Analogous structures exist on the Earth formed with water as the working fluid (Svensen et al., 2003). Whether such a process would work on Titan and what would be the underlying energy source in the crust of Titan require detailed modeling beyond the scope of this paper; we suggest this as a possible explanation for a population of circular structures worthy of further investigation.

The T8 swath also includes numerous roundish structures with bright edges with diameters of 10–80 km. There is no distinctive morphology that argues in favor of impact versus cryovolcanism as the origin of these larger features. If they are impact craters they are heavily weathered; arguments in favor of a cryovolcanic origin are hampered by the lack of apparent

flows exuded from the craters in contrast to similar features seen in the Ta swath (Elachi et al., 2005), with the exception of one possible flow associated with a large crater in T8 (Lopes et al., 2007).

4. Radiometry, altimetry, and relationship to Ta–T3 mapped units

4.1. Radiometry

Radiometry was obtained in all modes on T7 and T8. The radiometry independently addresses dielectric composition, surface and subsurface scattering properties, and is diagnostic of the relative roles of these properties in the radar appearance of different terrains. A broad region that was observed with combined scatterometry and radiometry in Ta (Elachi et al., 2005) was observed again in T8 in the orthogonal polarization. Advantage was taken of the very similar flyby geometries to observe the same region at nearly the same angles and resolutions. This region includes the eastern end of the T8 SAR swath, which contains the Huygens probe landing area.

The polarization of thermal emission from a surface can be interpreted in terms of its dielectric constant (Janssen et al., in preparation; Paganelli et al., 2007). The polarization is defined as

$$P(\theta) = (T_b(\text{parallel}) - T_b(\text{perp})) / (T_b(\text{parallel}) + T_b(\text{perp})),$$

where $T_b(\text{parallel})$ and $T_b(\text{perp})$ are the respective brightness temperatures parallel and perpendicular to the plane of incidence defined by the surface normal and the angle of emission θ . The polarization is conveniently independent of the absolute radiometric calibration, which is described for the Cassini radiometer by Janssen et al. (in preparation). It does depend on the stability of the relative radiometer calibration, which has been excellent ($\ll 1\%$ over hours and $\sim 1\%$ for two years since SOI), and on systematic errors with range due to antenna sidelobes, which are still under investigation but are expected to be insignificant in the present case.

The dielectric constant for a surface that is moderately rough on scales much larger than the wavelength can be retrieved from the polarization using the Fresnel equations and Kirchhoff's law (White and Cogdell, 1973). The result is not sensitive to subsurface scattering inasmuch as this tends to depolarize any related contributions without affecting the polarized surface emission; however, wavelength-scale roughness can lead to an underestimate of the dielectric constant by reducing the surface component (Paganelli et al., 2007). Fig. 4 shows a map of dielectric constant obtained from the Ta and T8 measurements made in the overlap region that contains the Huygens probe landing site. The area shown is that for which the dielectric constant can be reliably retrieved from the data; in particular, we include only angles of emission greater than 20 degrees where the signal comfortably exceeds the noise (the polarization goes to zero as normal incidence is approached), and less than about 60 degrees where the effect of large-scale roughness becomes a complicating factor. The resolution of the map is ~ 100 km,

which is the average beam 3 footprint width during the observations.

The dielectric constant retrieved in the neighborhood of the landing site is about 1.6. By itself, this suggests a surface of moderately compacted organic materials or very porous ($< 30\%$ density) water or ammonia ices. The Huygens probe result provides important ground truth. If this point is representative of the overall region, then one may conclude from the flat, lightly rubble-strewn image that roughness, particularly on the 2-cm wavelength scale, is not a strong factor, and that the surface is reasonably compact and hence composed of organic solids and liquids with very little ammonia or water ice.

Radiometry is also obtained in the SAR mode at much higher resolution (20 km and better), although at a single polarization. Paganelli et al. (2007) have shown a strong inverse correlation between the radar reflectivity (σ^0) and radiometric brightness in the sense that high radar reflection is associated with low radiometric brightness and, by inference, low emissivity, while low radar reflection is correspondingly associated with high radiometric brightness. The simplest explanation is that the reflectivity is caused largely by subsurface structure that produces volume scattering which, for a given dielectric constant, also results in reduced emissivity through Kirchhoff's law. We cannot rule out a surface phenomenon being responsible for the inverse relationship, but if we assume volume scattering, then areas of high emissivity could be characterized by a simpler dielectric structure such as infilling of organic material or aeolian deposits (dunes). For example the dark area at the poleward end of T7 shows lower normalized radar return and a brightness temperature a few degrees higher than is observed for the bright (possibly hilly) regions closer to the equator.

The T8 swath shows similar radiometric behavior for the dune area relative to the radar-bright areas. This leads to the possibility that the dark, embayed, terrain of T7 might be a dry, or largely dry, basin with infilling of organic material similar in composition and dielectric properties to the dunes, perhaps the reservoir of fine particulate material that is swept away and accumulated in the aeolian deposits mainly observed in the equatorial region of T8 and T3 as suggested by Paganelli et al. (2007).

4.2. Scatterometry

Low-resolution radar reflectivity (scatterometer) data were recorded on both T7 and T8 passes, however the T7 data were in a compressed format that is not well calibrated. Data acquired on the inbound segment of T8 overlap significantly with the inbound pass of Ta, and reproduce it closely. Fits to scattering models consist of a Hagfors-like specular term, which fits the surface scattering better than a Gaussian term, plus a \cos^n diffuse component representing diffuse scatter, which could be from surface or subsurface effects (Wye et al., 2007). The result is a dielectric constant of 1.95 ± 0.17 and a surface roughness of $5.28 \pm 1.2^\circ$ rms slope inbound, and a dielectric constant of 2.13 ± 0.13 with an rms slope of $7.67 \pm 1.6^\circ$ outbound. These values are somewhat higher than the values obtained through radiometry, as is often the case for the two techniques (Wye

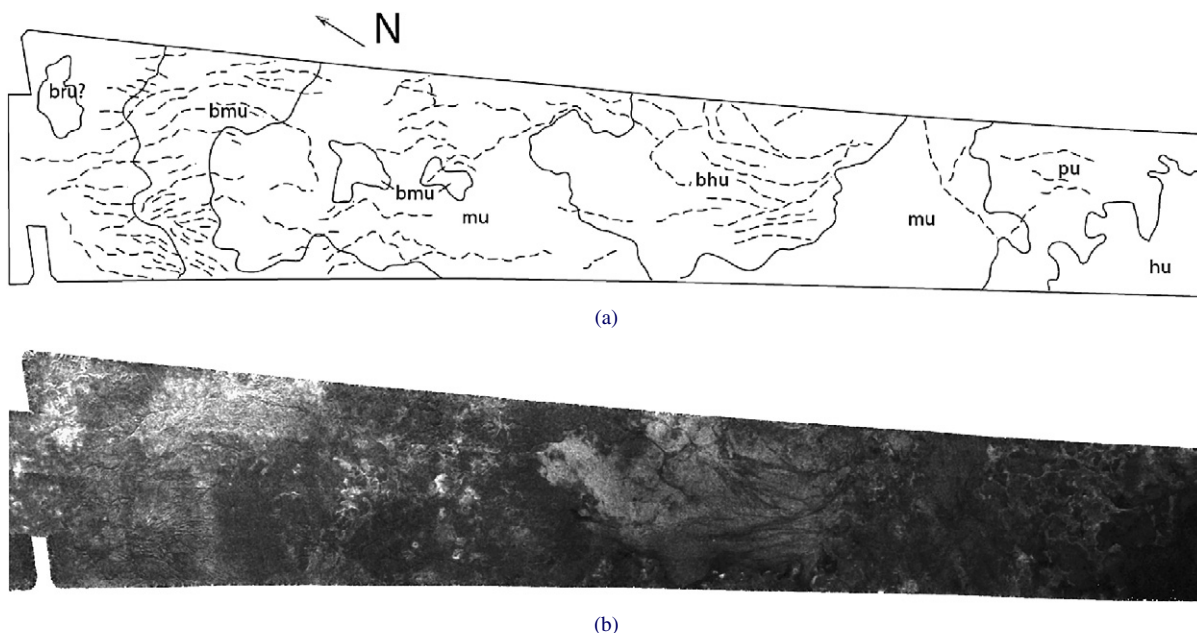


Fig. 5. (a) A map covering an approximately 700 km long region near the southeastern end of the T7 swath. Units mapped include the mottled unit, homogeneous unit, bright mottled unit, bright rough unit and patchy unit. Preliminary assignment of mapping units to T7. Key: bhu = bright homogeneous unit, bmu = bright mottled unit, brq = bright rough unit, hu = homogeneous unit, mu = mottled unit, and pu = plains unit. Properties of all but the last of these, which was not previously seen, are reported in Stofan et al. (2006). The dashed lines indicate the location of channels. (b) Portion of the T7 swath covered in the map. The swath is centered at 351.3° W, 56.2° S.

et al., 2007). The scatterometric dielectric constant is too low for all but the least consolidated water ice, and more consistent with mixtures of organic materials or even CO_2 ice (Wye et al., 2007). Surface diffuse scattering might lead to our underestimating the dielectric constant; however, while such scattering at centimeter and meter scales are likely prevalent on the surface, as suggested by the 1–10 cm-sized stones observed with the Huygens probe (Tomasko et al., 2005), the large magnitude of the diffuse scatter term at Titan appears to be more consistent with volume-scatter mechanisms than rough-surface models. From their data, Wye et al. (2007) cannot definitively say that multiple scattering from the subsurface dominates that from the surface, but they conclude that it is a strong possibility.

4.3. Altimetry

4.3.1. Altimetry

Altimetry measurements for T7 were lost due to an on-board recorder anomaly, but altimetry data were successfully collected both before and after the T8 SAR pass.

The T8 inbound altimetry swath spans approximately from 170 to 180° W, almost exactly on the equator. It lies in the infrared-dark region Shangri-La, about 700 km north-east of the Huygens landing site. The outbound pass is also very close to the equator, extending from 310 to 320° W, and is located in another dark region, Senkyo. No regional slopes or large-scale features are evident, and the variation of topographic heights along the ground track is modest, with a standard deviation of 20–30 m in both topographic profiles, which were respectively 400 and 500 km long. This value is comparable to the 30 m vertical resolution of the altimeter. For comparison, Schenk and Pappalardo (2004) report a standard deviation of 77 m over a

200 km long topographic profile across Conamara Chaos on Europa. Values of 10–20 m for the standard deviation over 30 km-long topographic profiles are typical for the Vastitas Borealis formation on Mars (e.g., Orosei et al., 2003).

Most of Shangri-La, as well as Belet, is covered by large fields of longitudinal sand dunes, with typical spacing of a few km and heights of 100–150 m (Lorenz et al., 2006). Topographic profiles across such dunes would have a standard deviation of the order of 50 m, but because the altimeter echo averages the topography over an area which is at least 20 km across the footprint-to-footprint height variation along the ground track of the altimeter is probably inadequate to derive the rms height of any dunes existing in the observed area.

Preliminary work to use range-centroid correction in the SAR data to obtain elevation changes along the SAR swaths themselves suggest a progressive downward trend in elevation from the equatorial to the polar end of the T7 swath (Stiles et al., in preparation).

4.4. Relationship of T7 and T8 areas to mapped units in Ta and T3

The bulk of the T7 swath (Fig. 5) consists of a unit with a variable radar appearance, similar to the mottled unit seen in the Ta and T3 swaths (Stofan et al., 2006). This unit has been interpreted to be a “plains” unit of unknown origin, likely largely composed of a spatially varying mixture of ice and organics. The hilly bright terrain at the equatorward end of the T7 swath is mapped as a bright rough unit, also present in the T3 swath. In the center of the swath, a bright mottled unit and a bright homogeneous unit are mapped, and again are seen in the T3 swath. The scalloped edge unit near the southern end of the swath is

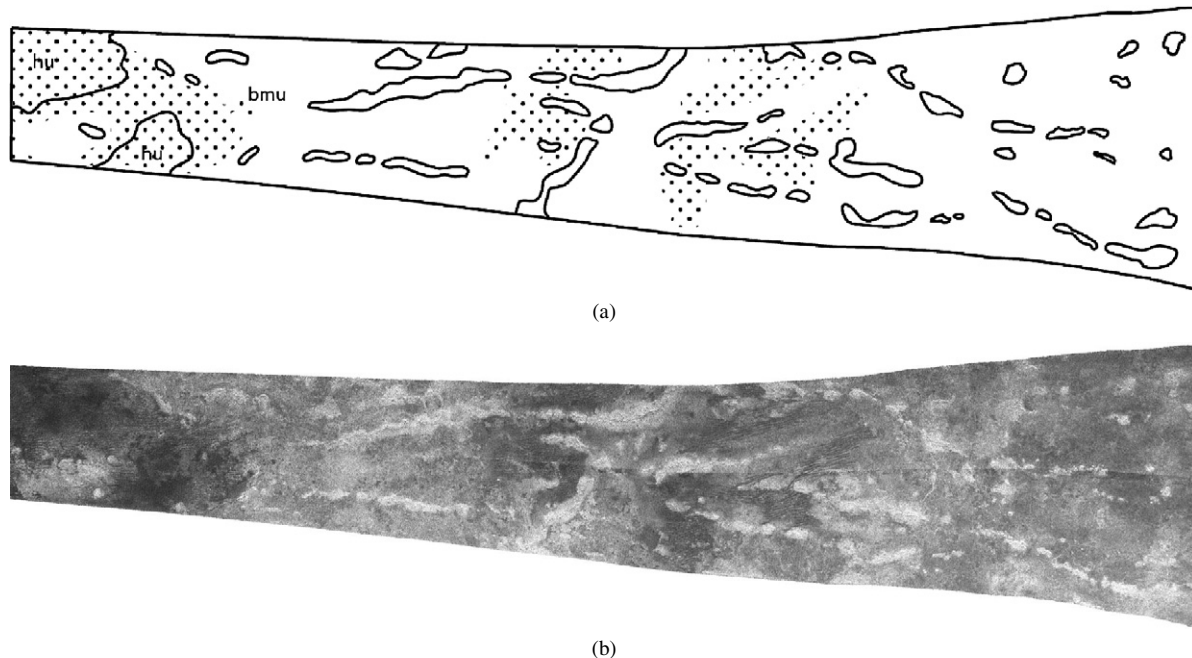


Fig. 6. (a) This map covers an approximately 1000-km-long segment of the T8 swath near its eastern end. The bulk of the area is mapped as the bright mottled unit, with small areas of the homogeneous unit at the western end. The stipple pattern marks the location of dunes; the unmarked units are the bright rough unit, demarking the position of hills. The pattern of the hills is suggestive of multiple orientations of long linear ridges, which have been subsequently eroded. North is to the top of the map. (b) Portion of the T8 swath covered by the map. The swath is centered at 144.6° W, 8.7° S.

mapped as a patchy unit, and has a morphology not seen previously in any other swath. The southern end of the swath is mapped as a homogeneous unit, similar to expanses of dark, relatively uniform terrain in Ta and T3, though this unit does appear to have lower backscatter.

The channels are confined to the region south of the small gaps in the T7 swath, and are superposed on the mottled unit, the bright mottled unit, the bright homogeneous unit and the patchy unit. In previous regions mapped (Stofan et al., 2006), channels tended to be more specifically located near geologic features, such as Ganesa Macula in Ta and Menrva Crater in T3. Mapping of channels in the T7 swath indicates their ubiquity over much of the swath, with the exception of the mottled plain-type unit at the northern end and the very dark homogeneous unit at the southern end. The lack of similarity of the patchy unit to other units, and its close association with the ‘shoreline’ and channels, is consistent with a topographically higher region that has been dissected and eroded by fluvial processes.

Mapping of the T8 region (Fig. 6) also reveals units seen in other regions of Titan. The central, radar-dark portion of the swath can be classified as the homogeneous unit identified in Stofan et al. (2006), bounded on the eastern and western sides by the bright mottled unit. Both of these units have superposed dunes. Both ends of the swath have linear to curvilinear, irregular outcrops of the bright rough unit, representing relatively higher terrain (the ‘mountains’ described above) that has either been extensively eroded and/or buried. The features at the western end of the swath are less distinct, and appear to be more degraded. It is possible that material derived from these hills, for example through one of or a combination of fluvial, rainfall, and aeolian erosion onto tectonically weakened ices,

provides much of the fine-grained debris found in the dunes. The chains of hills appear somewhat sinuous, more suggestive of features produced by compression than those produced by extension (Radebaugh et al., 2007). In the T8 case, the bright mottled unit does appear somewhat different than that mapped in other regions, in that it is predominantly composed of bright, patchy materials in close association with the linear hills. In this case, the mottling is likely due to variable roughness and extent of the blankets surrounding, and perhaps shed from, the hills.

In summary, mapping of the T7 and T8 swath reveals that much of the landscape covered in these radar swaths contains morphologic units similar to those mapped in earlier swaths, but with differences in their distributions and relationships. For example, patches of the bright rough unit were mapped in the T3 swath, but they do not form the more coherent sets of hills mapped in T8. We see no strong evidence of the cryovolcanic units of the Ta swath in T7 and T8, other than the enigmatic circular features discussed above. Additionally, dune fields in T8 are much more extensive and coherent than those seen in T3. The similarities between the basic morphologic units of the swaths suggest we are seeing regions formed by similar processes (aeolian, fluvial, cryovolcanic, limited tectonic), but the relative significance of each process varies, across different local and regional areas and perhaps over time.

5. The landing site of the Huygens probe seen in T8 radar data

Location of the Huygens probe’s landing site on Titan’s surface was accomplished by comparing the T8 radar image with the DISR image observations. The first step in this process was

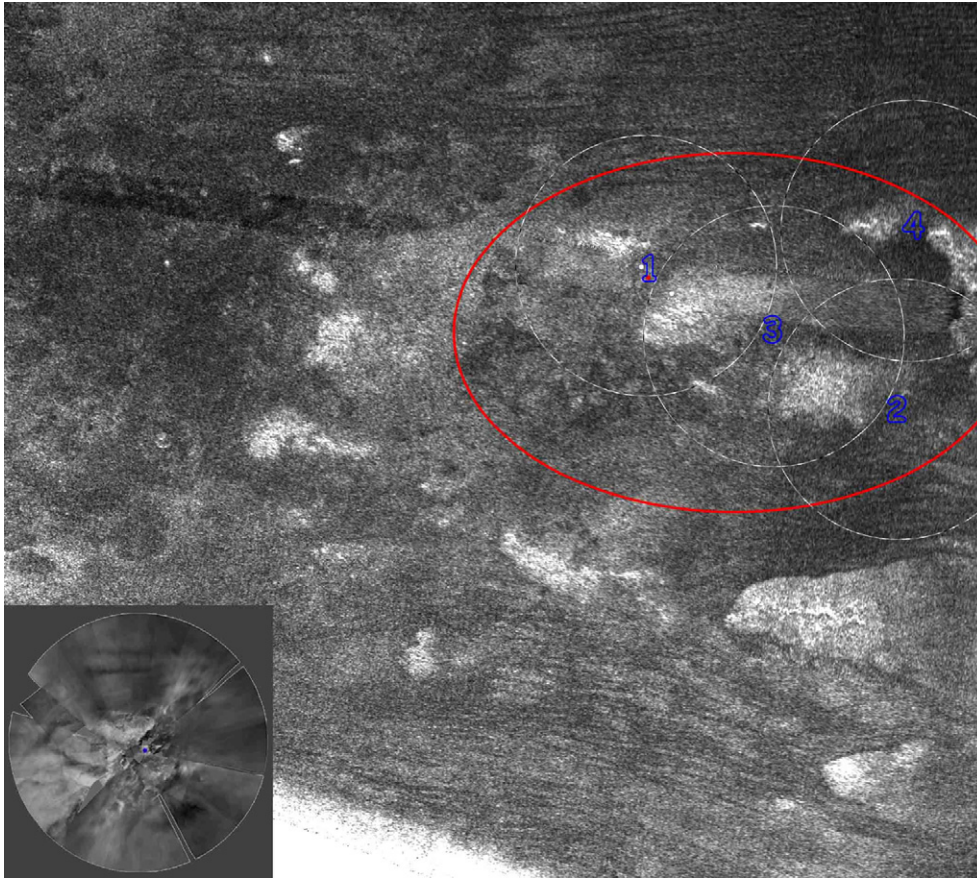


Fig. 7. An excerpt from the T8 radar swath overlaid with the calculated Huygens descent landing ellipse in red, and showing the four primary landing sites under consideration. The inset shows a mosaic of the DISR images stretched, projected and scaled to match the radar's image to be used for comparison of features. The excerpted part of the swath is centered at 165.3° W, 11.9° S.

to prepare a mosaic from the DISR images with the same projection and scale on Titan's surface as existed for the T8 radar swath. This mosaic is shown as an inset to Fig. 7. This circular area has a diameter of about 90 km on Titan's surface.

The next step was to constrain the area of potential landing sites by performing a dispersion analysis of the Descent Trajectory Working Group's (DTWG) calculation of the impact latitude and longitude. The DTWG analysis was primarily an integration of the measured probe accelerations for two cases: (1) from the atmosphere interface point at 1270 km (as determined by JPL) downward and (2) from Titan's surface upward. The lower trajectory was then tied to the upper trajectory near 150 km altitude. In the lower atmosphere wind measurements were also included in the analysis. The red ellipse in Fig. 7 shows the limits of the DTWG analysis dispersion.

Once the general area on the T8 swath had been determined a detailed search of this region was performed in an attempt to locate prominent features from the DISR mosaic on the T8 map. Several locations were evaluated, however the field was quickly reduced to 4 possible sites. These are shown by the numbers and ghost mosaic outlines in Fig. 7. The primary characteristic of interest was a dark colored area between lighter regions representing a possible southwest to northeast flow field. Site #1 is the best fit to the DISR data because of the matching of 4 additional prominent features: two horizontal features to the north

which we interpret as dunes, a circular feature near the top center, and the diagonal 'shoreline' near the center, as indicated in Fig. 8.

The Huygens probe's final resting place was determined on the mosaic via analysis of the DISR image progression to better than 100 m accuracy. Consequently its position can be subscribed on the radar swath thus indicating the probe's landing site. Fig. 9 shows the T8 radar swath overlaid with the DISR mosaic. Instrument sensitivity variations and geometric distortions degrade the registration accuracy between the DISR mosaic and radar map to perhaps a few kilometers. It is hoped that the accuracy will be improved using data from future encounters. The resulting coordinates for the Huygens landing site are 192.4° W longitude and -10.2° N latitude (that is, south of the equator) to an accuracy of about 0.1° .

The Huygens landing site is quite bright in T8 radar data, consistent with the ubiquitous presence in the DISR images of the landing site of centimeter- to 10 cm-sized pebbles (Tomasko et al., 2005). Thus the Huygens plains is a distinct unit from the plains or basin at the high latitude end of T7, in that the latter must be devoid of such materials. The two linear features that appear to be dunes are about 30 km from the landing site, and their distinctive presence in the radar images allows estimates of the atmospheric opacity to be made from the DISR images, where they are much less evident (Soderblom et al., 2007).

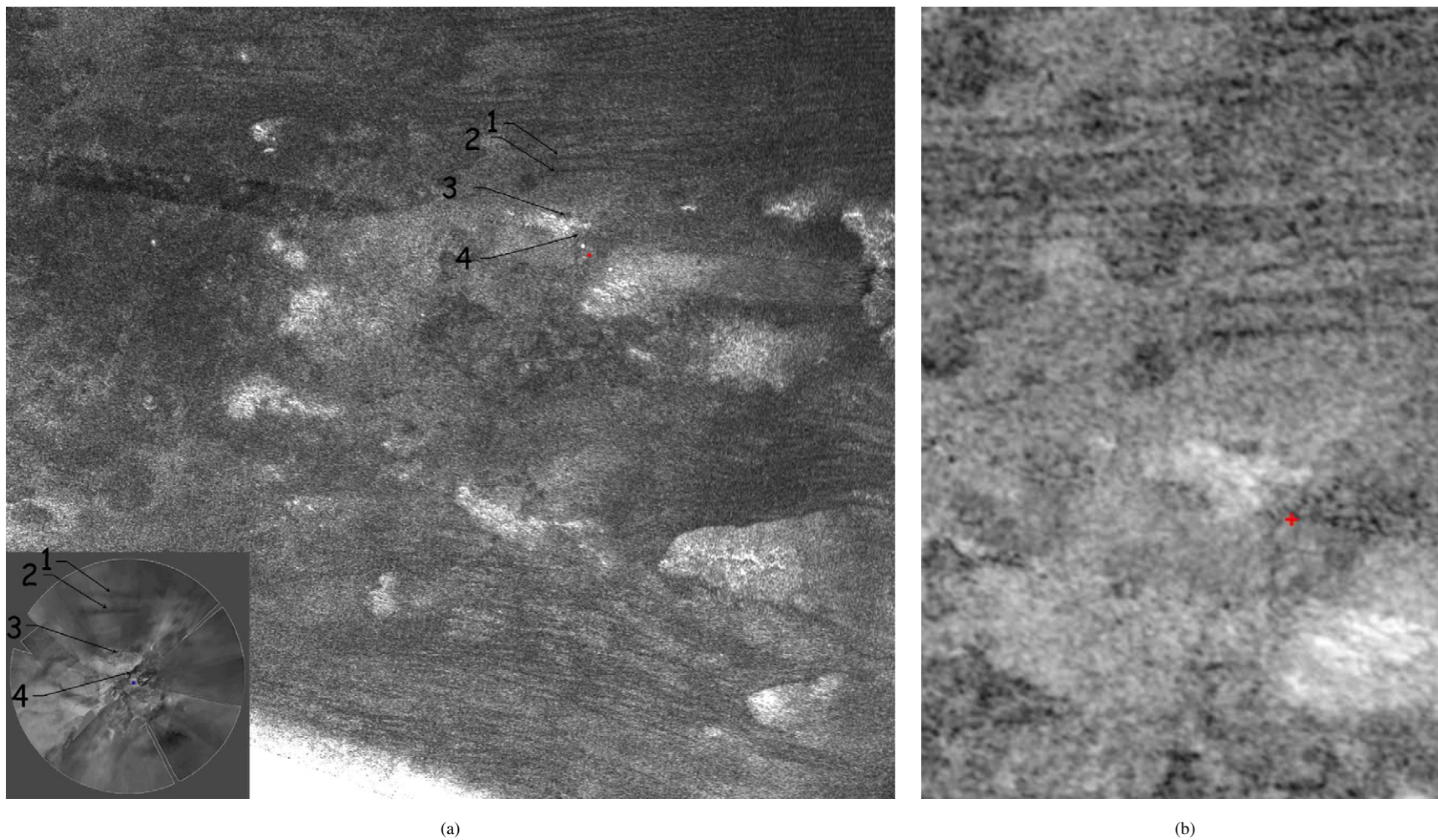


Fig. 8. (a) Similar to Fig. 7, but detailing the matching features from the radar and DISR data that were used in the final determination of the landing site of the Huygens probe. The excerpted part of the swath is centered at 166.5° W, 11.5° S. (b) Closeup of the final landing site location, with the adjacent bright hills and the two dunes 30 km to the north of the site clearly visible. Coordinates for the landing site location are in the text.



Fig. 9. An overlay of the DISR and Radar data showing the location of the Huygens probe landing site. The image is centered at 165.9° W, 11.9° S.

More detailed comparisons with VIMS and DISR data are hampered somewhat by the fact that the landing site appears near the end of the SAR swath, and therefore suffers from limited resolution and higher noise. Nonetheless, it is clear that the landing site is geologically distinct from the nearby edge of the widespread dune fields, and is characterized by processes that have deposited much larger sized debris on the plains than is represented in the radar-dark dunes (Soderblom et al., 2007).

6. Interpretations and unresolved questions for future observations

The two areas on Titan covered by the T7 and T8 passes are very different from each other, and underscore the strong diversity of Titan's landscapes. T7 imaged an area where liquids have dissected or are dissecting a landscape that likely has an overall decline in elevation toward the South Pole. The dark, almost featureless area nearest the pole lacks visible duneforms, is slightly brighter than the northern mid-latitude dunes, and is significantly brighter than the best candidates for present-day

basins of methane–ethane liquids in the high northern latitudes. Whether the southern plain is covered by a thin (meters to 10 m) hydrocarbon (methane or ethane) liquid, or represents the equatorward edge of solid substances that are poorly represented in mid-latitude dune fields and other dark areas, is unclear. Some or many of the organic products of Titan's photochemistry might preferentially condense out at the higher latitudes so there would be a tendency over time to accumulate solids of these products near the poles (Rannou et al., 2006), although some or all of these may gradually be transported equatorward. If the polar temperatures are several degrees below the equatorial value of approximately 94 K (Lorenz et al., 2001), methane will preferentially rain out seasonally at the poles as well, consistent with the broad geographic distribution of lakes and seas above 70° north latitude (Stofan et al., 2007; Mitri et al., 2007). The fine fluvial features seen toward the equatorial end of the pass and the more amorphous broad channels at higher southern latitudes may also play a role in feeding liquid to the dark region, though in the absence of a rainfall rate it is difficult to predict how much. In either case, it is likely that

the high-latitude, dark region of T7 is a unique unit not seen at lower latitudes. If the equivalent of the northern hemisphere lakes and seas exist above 70° south latitude, as hinted by one such feature seen in ISS data (Porco et al., 2005), it will be interesting to see whether the transition between the T7 dark region and individual lakes is a gradual one, or is sharp.

The T8 landscape illustrates two important points about Titan surface processes. First, while dunes appear at higher latitudes, in the areas imaged by the Cassini RADAR to date, they occur in irregular patches and clusters rather than as the extensive equatorial “seas” of dunes observed in T8 (Lorenz et al., 2006)—perhaps because of a relative lack of sand-sized particles or of the appropriate wind fields. Second, the overall lack of significant (>1 km amplitude) topography and appearance of subdued features hints either at a thin crust or deep burial of features over large areas of the T8 swath.

Suppose Titan’s surface were, on average, roughly 1/2–1 billion years old, based on the small number of identified impact craters (Lorenz et al., 2007). Photochemical models predict that the solid component of the stratospheric photochemical debris produced over geologic time (that is, excluding the ethane which is liquid under current Titan conditions) is equivalent to a globally averaged layer only 100–200 m thick (e.g., Wilson and Atreya, 2004). If we assume that large-scale resurfacing events that have acted to erase craters formed prior to a billion years ago also mixed some of this solid photochemical debris into the ice crust, then the amount of photochemical sediment available to bury geologic features might be less than 100 m thick, globally averaged, at present. The radarclinometric height of the mountains in T8 exceeds a kilometer, and approaches 2 km, in some places (Radebaugh et al., 2007); the topographic amplitude of the structures in total might not be much more than this because of the limited amount of photochemical debris. Thus the mountains on Titan are quite different from, for example, the basin and range structures in the southwestern part of North America, whose bulk is buried under kilometers of sediments, unless there were another source of sediments from, for example, very extensive fluvial erosion or extensive volcanic deposits. For example, Fortes et al. (2007) have proposed that the surface is buried under a thick layer of sediments produced by the cryogenic equivalent of pyroclastic ash, composed mostly of water ice but with ammonium sulfate as well. The many sharp boundaries between terrains argue, however, against thick burial.

The thermal evolution model of Tobie et al. (2006) posits a thin (10 km or less) crust for much of Titan’s history, maintained by the insulating and high-viscosity properties of methane clathrate hydrate, and thickening to 60 km only in the last ~500 million years as declining heat flows encourage the formation of normal ice I. Only features of order this age or less will exhibit significant topographic amplitude, and thus we may have an age constraint on the mountain chains in the T8 region consistent with other considerations (Radebaugh et al., 2007).

Future Cassini RADAR opportunities will include a number of flybys at high southern latitudes, although the precise area imaged in T7 will not be overflown again. Understanding the nature of the dark southern hemisphere terrain will thus de-

pend on coverage obtained at other longitudes and comparable, or greater, latitudes. Whether very dark “lakes” akin to those in the north are embedded within this terrain is an outstanding question that Cassini RADAR might answer. With respect to resolving the question of impact, cryovolcanic, or other origin of the circular features in T8, stereo imaging of features obtained by passing over the region at a different illumination azimuths may help elucidate the nature of these features. Higher resolution coverage of the Huygens site—300 m instead of a kilometer—will also be of keen interest, although this will not be obtained in the prime mission. Additional radiometry and scatterometry may ultimately decide between a surface covered by a relatively thin layer of organic sediments (much of which might be in the dune seas) and a thick layer of “cryoclastic” ash composed of water, sulfur and ammonia.

More broadly, the diverse terrains seen in T7 and T8 whet the appetite for more powerful radar systems or—in the long-term—a balloon-borne payload that would obtain Huygens-resolution near-infrared imaging (1–10 m) over large swaths of Titan’s surface (Lorenz et al., 2005; Tokano and Lorenz, 2006).

Acknowledgments

This work was supported by the Cassini Project through the various national funding agencies involved in the mission. We thank Robert Peckyno for computing the latitudes and longitudes of the images, as well as Paul Schenk and an anonymous referee for useful comments. We are grateful to the engineering team that flies the Cassini Orbiter and flew the Huygens Probe for their extraordinary expertise. The first author was a visiting professor at the Istituto di Fisica dello spazio Interplanetario in Rome, Italy, during much of the preparation of this work and is grateful to its director Dr. Angioletta Coradini for her hospitality and support.

References

- Elachi, C., Wall, S., Allison, M., Anderson, Y., Boehmer, R., Callahan, P., Encrenaz, P., Flamini, E., Francescetti, G., Gim, Y., Hamilton, G., Hensley, S., Janssen, M., Johnson, W., Kelleher, K., Kirk, R., Lopes, R., Lorenz, R., Lunine, J., Muhleman, D., Ostro, S., Paganelli, F., Picardi, G., Posa, F., Roth, L., Seu, R., Shaffer, S., Soderblom, L., Stiles, B., Stofan, E., Vetrilla, S., West, R., Wood, C., Wye, L., Zebker, H., 2005. First views of the surface of Titan from the Cassini RADAR. *Science* 308, 970–974.
- Elachi, C., Wall, S., Janssen, M., Stofan, E., Lopes, R., Kirk, R., Lorenz, R., Lunine, J., Paganelli, F., Soderblom, L., Wood, C., Wye, L., Zebker, H., Anderson, Y., Ostro, S., Allison, M., Boehmer, P., Callahan, P., Encrenaz, P., Flamini, E., Francescetti, G., Gim, Y., Hamilton, G., Hensley, S., Johnson, W., Kelleher, K., Muhleman, D., Picardi, G., Posa, F., Roth, L., Seu, R., Shaffer, S., Stiles, B., Vetrilla, S., West, R., 2006. Titan Radar Mapper observations from Cassini’s T₃ flyby. *Nature* 441, 709–713.
- Fortes, A.D., Grindrod, P.M., Trickett, S.K., Vocablo, L., 2007. Ammonium sulfate on Titan: Possible origin and role in cryovolcanism. *Icarus* 188, 139–155.
- Fulchignoni, M., Angrilli, F., Bianchini, G., Colombatti, G., Ferri, F., Lion Stoppato, P.F., Seiff, A., Zarnecki, J.C., McDonnell, J.A.M., Leese, M.R., Withers, P., Townner, M.C., Hathi, B., Harri, T., Mäkinen, A.M., Grand, R., Hamelin, M., Schwingenschuh, K., Lopez-Moreno, J.J., Rodrigo, R., Falkner, P., Svedhem, H., Jernej, I., Trautner, R., Bar-Nun, A., Barucci, A., Borucki, W., Coradini, M., Coustenis, A., Flamini, E., Gaborit, V., McKay,

- C.P., Neubauer, F., Tokano, T., Pirronello, V., 2005. Titan's physical characteristics measured by the Huygens Atmospheric Structure Instrument (HASI). *Nature* 438, 785–791.
- Kirk, R.L., Archinal, B.A., Tomasko, M.G., Rizk, B., Soderblom, L.A., Cook, D.A., Howington-Kraus, E., Becker, T.L., Rosiek, M.R., and the DISR Science Team, 2005. Topographic mapping of the Huygens landing site on Titan. *Bull. Am. Astron. Soc.* 37. Abstract 46.08.
- Lopes, R., Mitchell, K.L., Stofan, E.R., Lunine, J.I., Lorenz, R., Paganelli, F., Kirk, R.L., Wood, C.A., Wall, S.D., Robshaw, L.E., Fortes, A.D., Neish, C.D., Radebaugh, J., Reffet, E., Ostro, S.J., Elachi, C., Allison, M.D., Anderson, Y., Boehmer, R., Boubin, G., Callahan, P., Encrenaz, P., Flamini, E., Francescetti, G., Gim, Y., Hamilton, G., Hensley, S., Janssen, M.A., Johnson, W.T., Kelleher, K., Muhleman, D.O., Ori, G., Orosei, R., Picardi, G., Posa, F., Roth, L.E., Seu, R., Shaffer, S., Soderblom, L.A., Stiles, B., Vetrilla, S., West, R.D., Wye, L., Zebker, H.A., 2007. Cryovolcanic features on Titan's surface as revealed by the Cassini Titan Radar Mapper. *Icarus* 186, 395–412.
- Lorenz, R.D., 2006. The rivers of Xanadu and beyond: Cassini RADAR observations of Titan fluvial geomorphology. In: AGU Fall Meeting. Abstract P11-A.
- Lorenz, R.D., Lunine, J.I., McKay, C.P., Withers, P.G., 2001. Titan, Mars and Earth: Entropy production by latitudinal heat transport. *Geophys. Res. Lett.* 28, 415–418.
- Lorenz, R.D., Zimmerman, W., Lunine, J.I., 2005. Post-Cassini exploration of Titan: Science goals, instrumentation and mission concepts. *Adv. Space Res.* 36, 281–285.
- Lorenz, R.D., Wall, S., Radebaugh, J., Boubin, G., Reffet, E., Janssen, M., Stofan, E., Lopes, R., Kirk, R., Elachi, C., Lunine, J., Paganelli, F., Soderblom, L., Wood, C., Wye, L., Zebker, H., Anderson, Y., Ostro, S., Allison, M., Boehmer, R., Callahan, P., Encrenaz, P., Ori, G.G., Franceschetti, G., Gim, Y., Hamilton, G., Hensley, S., Johnson, W., Kelleher, K., Muhleman, D., Picardi, G., Posa, F., Roth, L., Seu, R., Shaffer, S., Stiles, B., Vetrilla, S., Flamini, E., West, R., 2006. The sand seas of Titan: Cassini RADAR observations of longitudinal dunes. *Science* 312, 724–727.
- Lorenz, R.D., Wood, C.A., Lunine, J.I., Wall, S.D., Lopes, R.M., Mitchell, K.L., Paganelli, F., Anderson, Y.Z., Wye, L., Tsai, C., Zebker, H., Stofan, E.R., and the Cassini Radar Team, 2007. Titan's young surface: Initial impact crater survey by Cassini RADAR and model comparison. *Geophys. Res. Lett.* 34, doi:10.1029/2006GL028971. L07204.
- Lunine, J., Artemieva, N., Lorenz, R., Flamini, E., 2005. Numerical modeling of impact cratering on Titan with implications for the age of Titan's surface. *Lunar Planet. Sci.* 36. Abstract 1504.
- Mitchell, K.L., Pallou, P., Stiles, B.W., Zebker, H., Mitri, G., Lunine, J.I., Wall, S.D., Lorenz, R.D., Lopes, R.M.C., Hensley, S., Stofan, E.R., Kirk, R.L., Ostro, S.J., Paganelli, F., and the Cassini Radar Team, 2007. Are Titan's lakes liquid filled? *Lunar Planet. Sci.* 38. Abstract 2081.
- Mitri, G., Showman, A.P., Lunine, J.I., Lorenz, R.D., 2007. Hydrocarbon lakes on Titan. *Icarus* 186, 385–394.
- Niemann, H.B., Atreya, S.K., Bauer, S.J., Carignan, G.R., Demick, J.E., Frost, R.L., Gautier, D., Haberman, J.A., Harpold, D.N., Hunten, D.M., Israel, G., Lunine, J.I., Kasprzak, W.T., Owen, T.C., Paulkovich, M., Raulin, F., Raaen, E., Way, S.H., 2005. The composition of Titan's atmosphere from the GCMS on the Huygens probe, and implications for the origin of nitrogen and methane. *Nature* 438, 779–784.
- Orosei, R., Bianchi, R., Coradini, A., Espinasse, S., Federico, C., Ferriccioni, A., Gavrishin, A.I., 2003. Self-affine behavior of martian topography at kilometer scale from Mars Orbiter Laser Altimeter data. *J. Geophys. Res. Planets* 108, 4-1.
- Paganelli, F., Janssen, M.A., Stiles, B., West, R., Lorenz, R.D., Lunine, J.I., Wall, S.D., Callahan, P., Lopes, R.M., Stofan, E., Kirk, R.L., Johnson, W.T.K., Roth, L., Elachi, C., and the Radar Team, 2007. Titan's surface from Cassini RADAR SAR and high resolution radiometry data of the first five flybys. *Icarus* 191, 211–222.
- Porco, C.C., and 35 colleagues, 2005. Imaging of Titan from the Cassini spacecraft. *Nature* 434, 159–168.
- Radebaugh, J., Lorenz, R., Kirk, R., Lunine, J., Stofan, E.R., Lopes, R., Wall, S., and the Cassini Radar Team, 2007. Mountains on Titan observed by Cassini Radar. *Icarus* 192, 77–91.
- Radebaugh, J., Lorenz, R., Lunine, J., Wall, S., Boubin, G., Reffet, E., Kirk, R., Lopes, R., Stofan, E., Soderblom, L., Allison, M., Janssen, M., Paillou, P., Callahan, P., and the Cassini Radar Team, 2008. Dunes on Titan observed by Cassini Radar. *Icarus*, doi:10.1016/j.icarus.2007.10.015, in press.
- Rannou, P., Montmessin, F., Hourdin, F., Lebonnois, S., 2006. The latitudinal distribution of clouds on Titan. *Science* 311, 201–205.
- Schenk, P.M., Pappalardo, R.T., 2004. Topographic variations in chaos on Europa: Implications for diapiric formation. *Geophys. Res. Lett.* 31, doi:10.1029/2004GL019978.
- Sears, W.D., 1995. Tidal dissipation in oceans on Titan. *Icarus* 113, 39–56.
- Soderblom, L.A., Tomasko, M.G., Archinal, B.A., Becker, T.L., Bushroo, M.W., Cook, D.A., Doose, L.R., Galuszka, D.M., Hare, T.M., Howington-Kraus, E., Karkoschka, E., Kirk, R.L., Lunine, J.I., McFarlane, E.A., Redding, B.L., Rizk, B., Rosiek, M.R., See, C., Smith, P.H., 2007. Topography and geomorphology of the Huygens landing site on Titan. *Planet. Space Sci.* 55, 2015–2024.
- Sotin, C., Jaumann, R., Buratti, B.J., Brown, R.H., Clark, R.N., Soderblom, L.A., Baines, K.H., Bellucci, G., Bibring, J.-P., Capaccioni, F., Cerroni, P., Combes, M., Coradini, A., Cruikshank, D.P., Drossart, P., Formisano, V., Langevin, Y., Matson, D.L., McCord, T.B., Nelson, R.M., Nicholson, P.D., Sicardy, B., LeMouelic, S., Rodriguez, S., Stephan, K., Scholz, C.K., 2005. Release of volatiles from a possible cryovolcano from near-infrared imaging of Titan. *Nature* 435, 786–789.
- Stofan, E., Lunine, J.I., Lopes, R., Paganelli, F., Lorenz, R., Wood, C., Kirk, R., Wall, S., Elachi, C., Allison, M.D., Anderson, Y., Boehmer, R., Boubin, G., Callahan, P., Elachi, C., Soderblom, L.A., Ostro, S., Janssen, M., Radebaugh, J., Wye, L., Zebker, H., Anderson, Y., Allison, M., Boehmer, R., Callahan, P., Encrenaz, P., Flamini, E., Francescetti, G., Gim, Y., Hamilton, G., Hensley, S., Johnson, W.T.K., Kelleher, K., Muhleman, D., Picardi, G., Posa, F., Roth, L., Seu, R., Shaffer, S., Stiles, B., Vetrilla, S., West, R., 2006. Mapping of Titan: Results from the first two radar passes. *Icarus* 185, 443–456.
- Stofan, E.R., Elachi, C., Lunine, J.I., Lorenz, R.D., Stiles, B., Mitchell, K.L., Ostro, S., Soderblom, L., Wood, C., Zebker, H., Wall, S., Janssen, M., Kirk, R., Lopes, R., Paganelli, F., Radebaugh, J., Wye, L., Anderson, Y., Allison, M., Boehmer, R., Callahan, P., Encrenaz, P., Flamini, E., Francescetti, G., Gim, Y., Hamilton, G., Hensley, S., Johnson, W.T.K., Kelleher, K., Muhleman, D., Paillou, P., Picardi, G., Posa, F., Roth, L., Seu, R., Shaffer, S., Vetrilla, S., West, R., 2007. The lakes of Titan. *Nature* 445, 61–64.
- Svensen, H., Planke, S., Jamtveit, B., Pedersen, T., 2003. Seep carbonate formation controlled by hydrothermal vent complexes: A case study from the Voring Basin, the Norwegian Sea. *Geo-Mar Lett.* 23, 351–358.
- Tobie, G., Lunine, J.I., Sotin, C., 2006. Episodic outgassing as the origin of atmospheric methane on Saturn's moon Titan. *Nature* 440, 61–64.
- Tokano, T., Neubauer, F.M., 2002. Tidal winds on Titan caused by Saturn. *Icarus* 158, 499–515.
- Tokano, T., Lorenz, R.D., 2006. GCM simulation of balloon trajectories on Titan. *Planet. Space Sci.* 54, 685–694.
- Tomasko, M., Archinal, B., Becker, T., Bézard, B., Bushroo, M., Combes, M., Cook, D., Coustenis, A., de Bergh, C., Dafeo, L., Doose, L., Douté, S., Eibl, A., Engel, S., Gliem, F., Grieger, B., Holso, K., Howington-Kraus, E., Karkoschka, E., Keller, H., Kirk, R., Kramm, R., Küppers, M., Lanagan, P., Lellouch, E., Lemmon, M., Lunine, J., McFarlane, E., Moores, J., Prout, M., Rizk, B., Rosiek, M., Rueffer, P., Schröder, S., Schmitt, B., See, C., Smith, P., Soderblom, L., Thomas, N., West, R., 2005. Rain, winds, and haze during the Huygens probe descent to Titan's surface. *Nature* 438, 765–778.
- White, T.L., Cogdell, J.R., 1973. Lunar polarization studies at 3.1 mm wavelength. *Moon* 6, 235–249.
- Wilson, E.H., Atreya, S., 2004. Current state of modeling the photochemistry of Titan's mutually dependent atmosphere and ionosphere. *J. Geophys. Res.* 109, doi:10.1029/2003JE002181. E06002.
- Wood, C.A., Lunine, J.I., Lopes, R.M., Stofan, E.R., Mitchell, K., Radebaugh, J., 2006. Crateriform structures on Titan. *Lunar Planet. Sci.* 37. Abstract 1659.
- Wye, L.C., Zebker, H.A., Ostro, S.J., West, R.D., Gim, Y., Lorenz, R.D., and the Cassini RADAR Team, 2007. Electrical properties of Titan's surface from Cassini RADAR scatterometer measurements. *Icarus* 188, 367–385.